

Electronic Supplementary Information

Diacetylene-bridged covalent organic framework as crystalline graphdiyne analogue for photocatalytic hydrogen evolution

Zhiqing Lin,^a Songyao Dai,^a Shan Yao,^b Qia-Chun Lin,^a Mengying Fu,^a Lai-Hon Chung,^{*a} Bin Han,^{*b} and Jun He,^{*a}

^aSchool of Chemical Engineering and Light Industry, Guangdong University of Technology, Guangzhou 510006, China. Email: junhe@gdut.edu.cn; laihonchung@gdut.edu.cn

^bGuangdong Basic Research Center of Excellence for Ecological Security and Green Development, Key Laboratory for City Cluster Environmental Safety and Green Development of the Ministry of Education, School of Ecology, Environment and Resources, Guangdong University of Technology, Guangzhou, 510006, P. R. China. Email: hanbin@gdut.edu.cn

Table of contents

Materials and characterization.....	3
Experimental procedures.....	7
Photocatalytic hydrogen generation experiment	27
References	44

Materials and characterization

All chemicals were obtained from commercial sources including 4-iodoaniline, triphenylphosphine (PPh₃), *trans*-dichlorobis(triphenylphosphine) palladium(II) (PdCl₂(PPh₃)₂), cuprous iodide (CuI), trimethylsilylacetylene (TMSA), 2,4,6-triformylphloroglucinol (Tp), 1,3,5-tribromobenzene, 1,4-Dioxane, Mesitylene, Methanol (MeOH), *N,N*-Dimethylformamide (DMF), dichloromethane (CH₂Cl₂), Triethanolamine (TEOA) and tetrahydrofuran (THF) and used without further purification. Elemental analysis was obtained with a VarioMicro CUBE CHN elemental analyzer. Powder X-ray diffraction (PXRD) patterns were collected on a Rigaku Smart lab diffractometer with Cu K α radiation ($\lambda = 1.5418 \text{ \AA}$) at room temperature. The X-ray tube was operated at a voltage of 40 kV and a current of 15 mA. Fourier transform infrared (FT-IR) spectra in the range 400–4000 cm⁻¹ were recorded on a Nicolet Avatar 360 FT-IR spectrophotometer. Nuclear magnetic resonance (NMR) spectra were recorded at 298 K on a 400 MHz Bruker superconducting magnet high-field NMR spectrometer, with working frequencies of 400 MHz for ¹H and 101 MHz for ¹³C nuclei. Chemical shifts (δ) are expressed in ppm relative to the residual solvent (*e.g.*, CDCl₃, ¹H: 7.26 ppm, ¹³C: 77.16 ppm) reference. Coupling constants are expressed in hertz. Thermogravimetric analysis (TGA) was carried out in a PerkinElmer thermal analysis equipment (STA 6000) with a heating rate of 10 °C/minute in N₂ atmosphere. Diffuse reflection spectra were collected in the UV-Visible Near Infra-Red Spectrophotometer with Integrating Sphere (Shimazu 3600 plus). The fluorescence spectra were measured using HORIBA Scientific Fluorolog-3. The porosity and surface area analysis were performed using a Quantachrome Autosorb iQ gas sorption analyzer. The electron paramagnetic resonance (EPR) spectra were recorded using a Bruker ER-420 spectrometer. The central magnetic field was 3350 G, and the modulation frequency was 100 kHz. The X-ray photoelectron spectroscopy (XPS) spectra were recorded on an ESCALAB 250 system. The optical power on the surface was measured by a power meter (CEL-NP2000-2A, Beijing Aulight Co. Ltd., China). Kelvin probe force microscopy (KPFM) data were collected at Bruker Dimension FastScan. The Raman spectra were recorded in ACCUMAN SR-510 Pro with continuous laser excitation (785 nm).

Electrochemical measurements.

Indium-tin oxide (ITO) glasses, platinum wire electrode and Ag/AgCl electrode (saturated KCl) were used as working electrode, assistant electrode and reference electrode, respectively. The electrolyte was a 0.2 M Na₂SO₄ aqueous solution (pH 6.8). 2 mg of COF powder was dispersed in 1 mL ethanol and ultra-sonicated for 30 min to get a slurry. After the addition of 10 μL Nafion, the mixture (loading: 100 μL) was spread onto ITO glass to get a regular-shaped membrane with an effective area of 1 cm². The photocurrent measurements were conducted with a CHI760e electrochemical workstation (CH Instrument, Shanghai, China), with the working electrodes irradiated from the front side. The visible light was generated by a 300 W xenon lamp (CEL-HXF300, Beijing China Education Au-light Co., Ltd) with a 420-nm cut-off filter, and was chopped manually. In addition, Mott-Schottky measurement and electrochemical impedance spectroscopy (EIS) measurement were performed in the dark under the same system. For Mott-Schottky measurements, the amplitude was 0.005 V with frequencies of 500, 800, and 1000 Hz. The applied potentials vs. Ag/AgCl were converted to normal hydrogen electrode (NHE) potentials using the following equation:

$$E (\text{vs. NHE}) = E (\text{vs. Ag/AgCl}) + 0.197 \text{ V}$$

Structure modelling. Structural modeling and Pawley refinement were carried out in the Materials Studio 2018 software package for crystal determination from the XRD pattern. The space groups were obtained from the Reticular Chemistry Structure Resource. The theoretical models were then optimized by the Forcite module. Pawley refinements of the PXRD patterns were performed in the Reflex module from 2° to 50°, which agree well with the simulated patterns of AA stacking models.

Photocatalytic H₂ evolution.

All photocatalytic experiments were performed by a multichannel photochemical reaction system in a 50-mL Pyrex reaction vessel, where the photoreaction temperature was kept at a constant temperature (25 °C) with circulating water. In the photocatalytic H₂ evolution reaction system, 5 mg as-synthesized polymer was ultrasonically dispersed in 10 mL DMF (dispersant) for 10 minutes. Then, 10 mL ascorbic acid (AA) aqueous solution (the concentration of AA in the mixed solution =

0.5 M) and 30 μL H_2PtCl_6 aqueous solution (Pt content: 3 wt.%) was added to form a 20 mL mixture solution, which was poured into the photo-reactor equipped with magnetic stirrer. Pt was loaded on the surface of the photocatalyst by *in situ* photo-deposition approach using H_2PtCl_6 . After sealing the reactor, reaction mixture was purged with Ar flow to remove air and illuminated with a visible light LED source ($\lambda_{\text{ex}} > 420$ nm). The produced hydrogen was measured by gas chromatography (Fuli GC9790Plus, argon as a carries gas) using a thermal conductivity detector (TCD). After the photocatalytic experiments, the photocatalysts were recovered by washing with water, ethanol before drying at 70 $^\circ\text{C}$.

Calculation of the Apparent Quantum Yield (AQY)

The apparent quantum yield (AQY) is a crucial parameter for assessing the apparent solar-to-hydrogen efficiency of the photocatalysts. The AQY for hydrogen evolution was measured with monochromatic light obtained by using bandpass filters of 365, 385, 420, 450, 485, 535, 595, 630, and 760 nm. (Beijing Perfect Light Technology Co., LTD., Beijing, China). The photocatalytic experiments were conducted following the same conditions as described above. The active area of the reactor is about 7.065 cm^2 . PL-MW2000 optical radiometer was used to take the average value of monochromatic light intensity at three representative points.

The AQY was calculated as below:

$$\eta = \frac{2 \times M \times N_A \times h \times c}{S \times P \times t \times \lambda} \times 100\%$$

Where M is the amount of the produced H_2 (mol), N_A is Avogadro constant ($6.022 \times 10^{23} \text{ mol}^{-1}$), h is the Planck constant ($6.626 \times 10^{-34} \text{ J}\cdot\text{s}$), c is the speed of light ($3 \times 10^8 \text{ m/s}$), S is the irradiation area of the incident light (cm^2), P is the intensity of incident light (W/cm^2), t is the photoreaction time (s), λ is the wavelength of the monochromatic light (m). According to the equation, the AQY is related to the intensity of incident light and the irradiation area. These parameters in different groups are possibly different, resulting in different AQYs.

Density functional theory (DFT) calculations.

All calculations of building blocks and **TP-COFs** model molecules were implemented in density functional theory (DFT) *via* Gaussian 16A software. The geometry optimization calculations and single-point calculations of the ground states were performed using the B3LYP functional coupled with a 6-31G (d) basis set for orbital analysis and electrostatic potential. The excited state electronic properties of **S2-TP COF** structured molecules were performed using time dependent density functional theory (TD-DFT) with B3LYP functional coupled with a 6-31G (d) basis set was utilized. Multiwfn 3.8^[S1] and VMD 1.9.3^[S2] programs were employed for analyzing orbital composition and visualizing the data, respectively. The isosurface value was set to be 0.02 a.u., with the red and blue region indicating positive and negative values of the orbitals respectively.

The Gibbs free energy change (ΔG_{H^*}) of the photocatalytic H₂ evolution reaction was expressed by the following equation:

$$\Delta G_{H^*} = \Delta E_{H^*} + \Delta E_{zpe} - T\Delta S$$

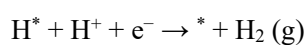
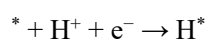
where ΔE_{H^*} is the DFT computed adsorption energy, ΔE_{zpe} and ΔS represent the zero-point energy difference and the entropy difference between the adsorbed state and the gas phase, respectively, and T is the system temperature (298.15 K). The entropy of the free molecule H₂ is taken from the NIST database.

The adsorption energy (ΔE_{H^*}) was calculated and defined as:

$$\Delta E_{H^*} = \Delta E_{\text{total}} + \Delta E_{\text{catalyst}} - E_{\text{H}_2}$$

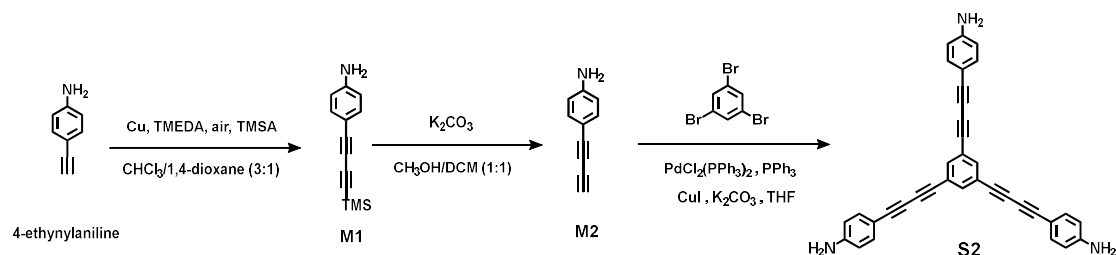
where ΔE_{total} , $\Delta E_{\text{catalyst}}$ and E_{H_2} correspond to the total energies of **S2-TP COF** model with adsorbed H species, **S2-TP COF** without adsorbed H species, and isolated species, respectively.

The HER process involves two-electron pathways, proton/electron transfer step and hydrogen release step:



where * denotes the adsorption site and H* denotes the adsorbed H atoms.

Experimental procedures



Scheme S1. The synthetic scheme for **S2**.

Synthesis of 4-ethynylaniline

The synthesis was carried out according to the literature.^[S3]

Synthesis of 4-((trimethylsilyl)buta-1,3-diyne-1-yl)aniline (**M1**)

M1 was synthesized according to the previously reported procedure.^[S4] To a solution of trimethylsilylacetylene (0.48 mL, 2 eq.) and 4-ethynylaniline (200 mg, 1.7 mmol) in 4 mL $\text{CHCl}_3/1,4\text{-dioxane}$ (3:1, v/v) were added Cu powder (5.4 mg, 5 mol%) and TMEDA (51 μL , 20 mol%). After the mixture was stirred for 20 hours at 50 °C, aqueous NH_4Cl solution was added and the mixture was extracted with CH_2Cl_2 , and washed with saturated NaCl solution. Finally, the crude product was concentrated under reduced pressure and then purified by column chromatography on silica gel (eluent: petroleum ether (PE)/ CH_2Cl_2 = 2:1, v/v) to give **M1** as a yellow compound (solid, yield: 60%). ^1H NMR (400 MHz, Chloroform-*d*) δ 7.29 (d, J = 8.5 Hz, 2H), 6.56 (d, J = 8.5 Hz, 2H), 3.89 (s, 2H), 0.22 (s, 9H). ^{13}C NMR (101 MHz, Chloroform-*d*) δ 147.95, 134.56, 114.87, 110.40, 89.75, 88.76, 78.36, 72.65, 0.00.

Synthesis of 4-(buta-1,3-diyne-1-yl)aniline (**M2**)

To a solution of **M1** (100 mg, 0.47 mmol) in 4 mL of $\text{CH}_2\text{Cl}_2/\text{MeOH}$ (1:1, v/v) was added K_2CO_3 (258.7 mg, 1.87 mmol). The mixture was stirred at room temperature for 2 hours and filtered at reduced pressure. Then H_2O was added to the filtrate and the mixture was extracted with CH_2Cl_2 . The organic phase was washed with H_2O and brine, dried over Na_2SO_4 , and then concentrated at

reduced pressure. The crude residue was used directly without further purification for the next step. ^1H NMR (400 MHz, Chloroform-*d*) δ 7.32 (d, $J = 8.6$ Hz, 2H), 6.58 (d, $J = 8.6$ Hz, 2H), 3.90 (s, 2H), 2.44 (s, 1H). ^{13}C NMR (101 MHz, Chloroform-*d*) δ 147.77, 134.39, 114.58, 109.81, 76.51, 71.70, 70.46, 68.71.

Synthesis of 4,4',4''-(benzene-1,3,5-triyltris(buta-1,3-diyne-4,1-diyl))trianiline (**S2**)

1,3,5-tribromobenzene (55 mg, 0.17 mmol), **M2** (148 mg, 6 eq.), CuI (1.66 mg, 0.05 eq.), PdCl₂(PPh₃)₂ (4.9 mg, 0.04 eq.), PPh₃ (4.6 mg, 0.1 eq.) and K₂CO₃ (144.7 mg, 6 eq.) were loaded into a 25-mL Schlenk tube. The mixture was evacuated and backfilled with N₂ three times followed by the addition of 4 mL THF under N₂ atmosphere. After stirring the solution at 65 °C for 24 hours, the solvent was removed under reduced pressure by a rotary evaporator. Finally, the mixture was purified by silica gel chromatography using PE/ethyl acetate (EA) (1:1, v/v) as eluent to give **S2** as yellow compound (light yellow solid, yield: 71%, based on 1,3,5-tribromobenzene) ^1H NMR (400 MHz, DMSO-*d*₆) δ 7.74 (s, 3H), 7.27 (d, $J = 8.5$ Hz, 6H), 6.55 (d, $J = 8.5$ Hz, 6H), 5.87 (s, 6H). ^{13}C NMR (101 MHz, DMSO-*d*₆) δ 151.45, 135.88, 134.57, 123.37, 114.06, 105.40, 86.31, 79.03, 76.87, 71.59.

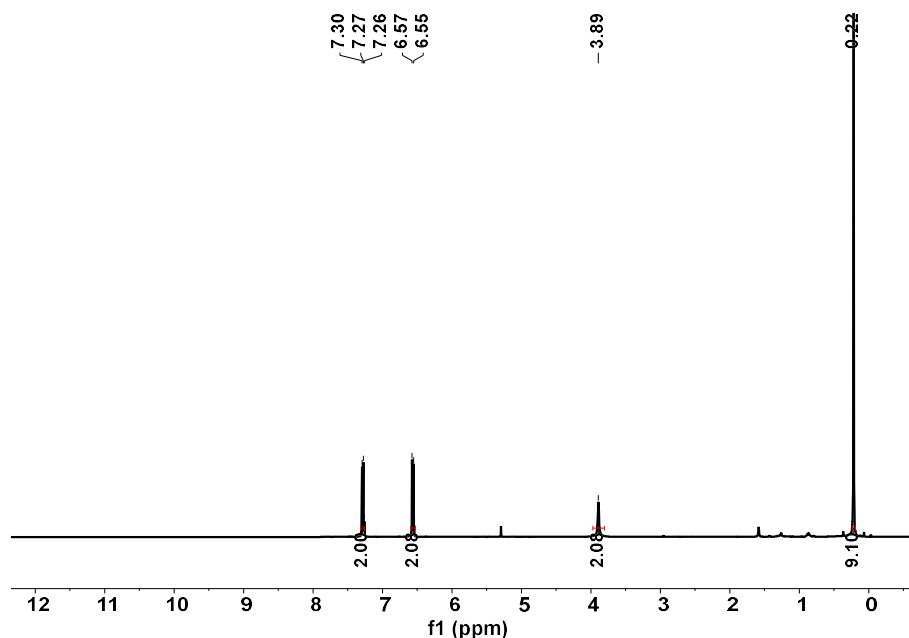


Figure S1. ^1H NMR spectrum of compound **M1** in CDCl₃.

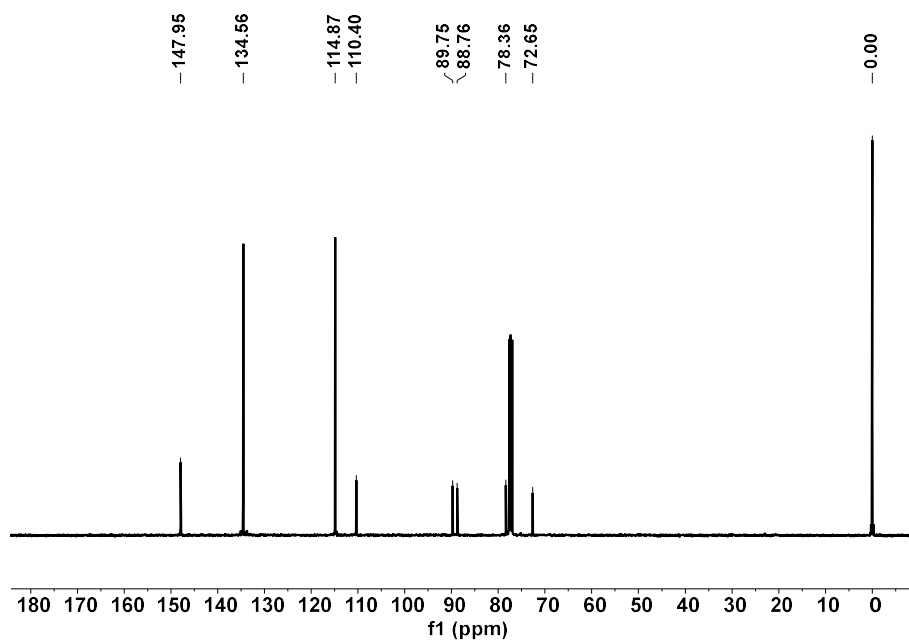


Figure S2. ^{13}C NMR spectrum of compound **M1** in CDCl_3 .

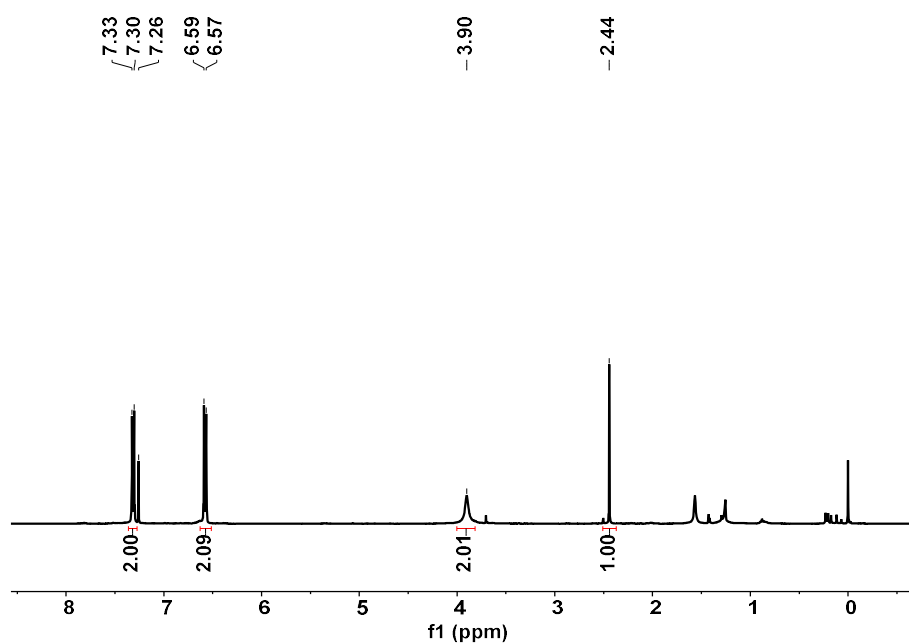


Figure S3. ^1H NMR spectrum of compound **M2** in CDCl_3 .

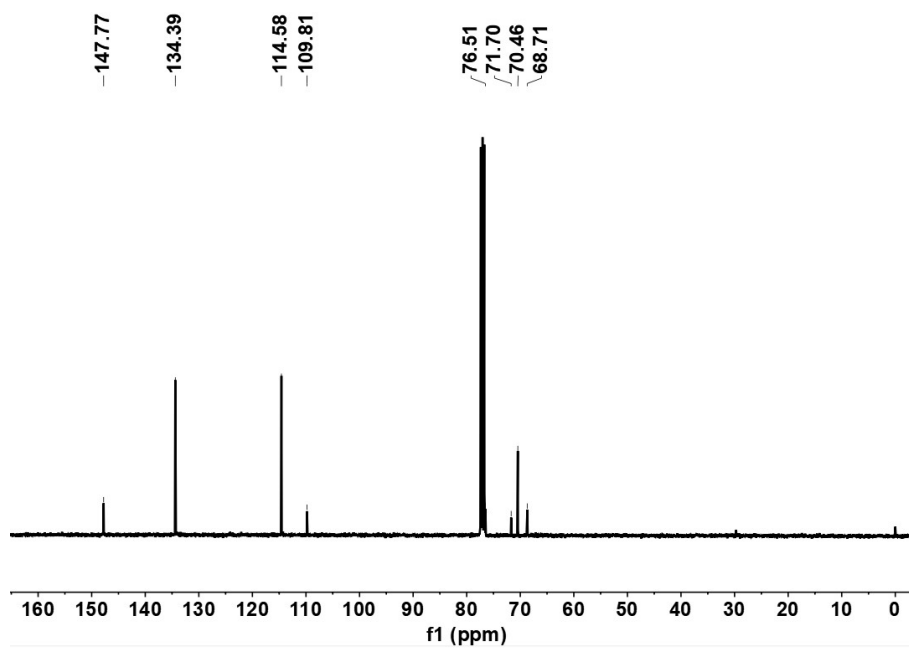


Figure S4. ^{13}C NMR spectrum of compound **M2** in CDCl_3 .

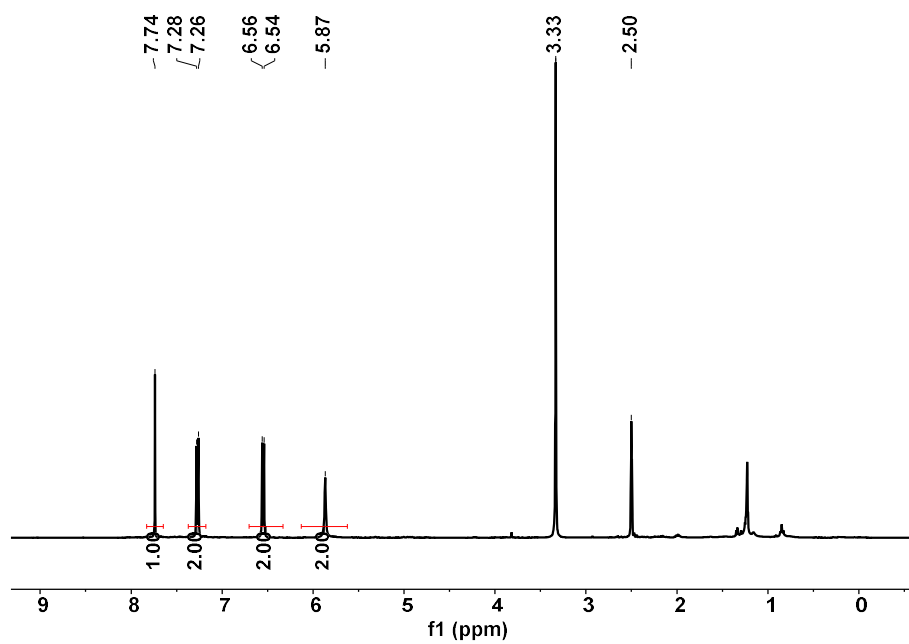


Figure S5. ^1H NMR spectrum of compound **S2** in $\text{DMSO}-d_6$.

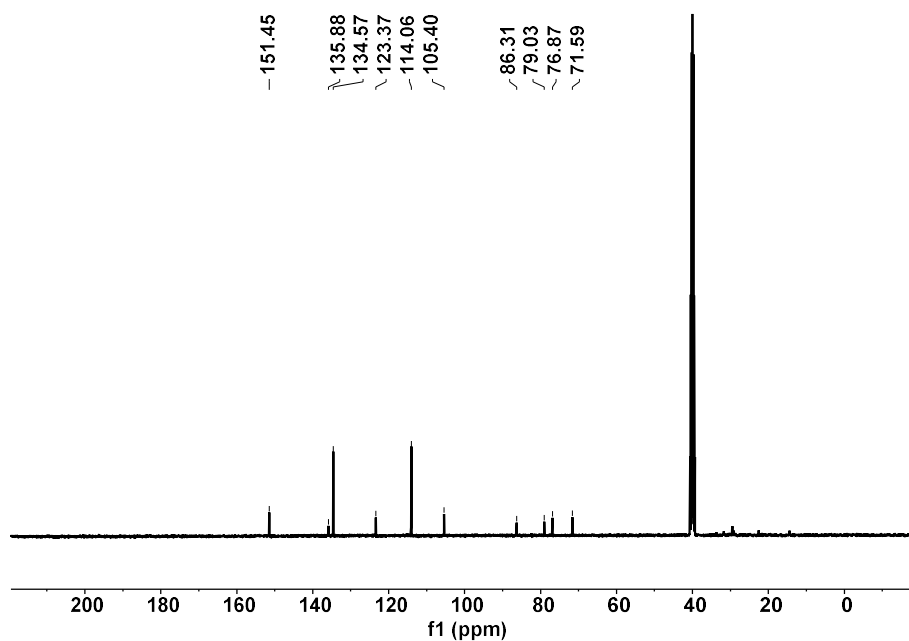
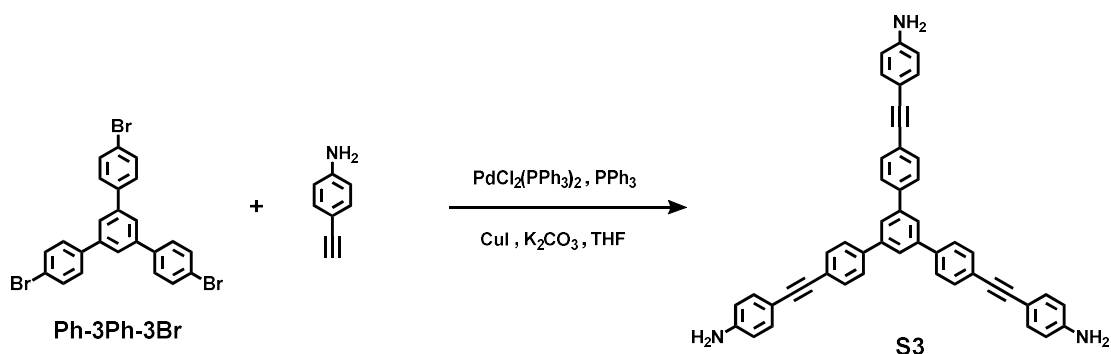


Figure S6. ^{13}C NMR spectrum of compound **S2** in $\text{DMSO-}d_6$.



Scheme S2. The synthetic scheme for **S3**.

Synthesis of **S5**

Ph-3Ph-3Br (400 mg, 0.737 mmol), 4-ethynylaniline (345 mg, 4 eq.), CuI (11.5 mg, 5 mol%), $\text{PdCl}_2(\text{PPh}_3)_2$ (20.7 mg, 4 mol%), PPh_3 (19.3 mg, 10 mol%) and K_2CO_3 (610 mg, 6 eq.) were loaded into a 25-mL Schlenk tube. The mixture was evacuated and backfilled by N_2 atmosphere for three cycles and then 6 mL THF was added under N_2 atmosphere. The reaction mixture was then stirred for 24 hours at 65 °C, and the solvent was then removed by rotary evaporation under reduced pressure. The mixture was purified by silica gel chromatography using PE/EA (1:2, v/v) as eluent to obtain the desired compound **S3**. (light yellow solid, yield: 85%, based on **Ph-3Ph-3Br**) ^1H NMR (400 MHz, $\text{DMSO-}d_6$) δ 7.97–7.87 (m, 9H), 7.58 (d, $J = 8.2$ Hz, 6H), 7.26 (d, $J = 8.3$ Hz, 6H), 6.60 (d,

$J = 8.4$ Hz, 6H), 5.60 (s, 6H). ^{13}C NMR (101 MHz, $\text{DMSO-}d_6$) δ 150.05, 141.33, 139.41, 133.14, 131.83, 127.81, 123.38, 114.18, 108.64, 92.87, 87.05.

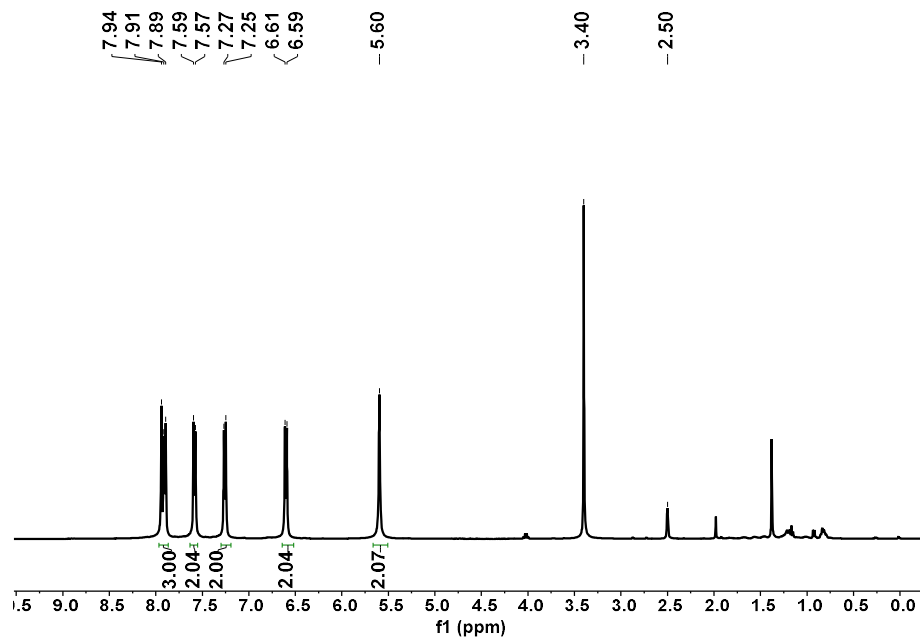


Figure S7. ^1H NMR spectrum of compound **S3** in $\text{DMSO-}d_6$.

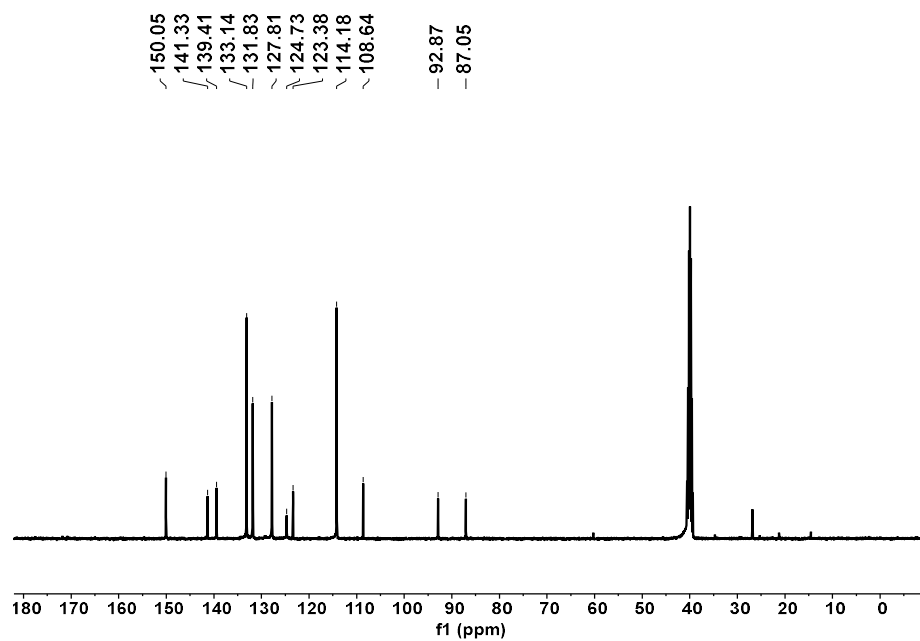
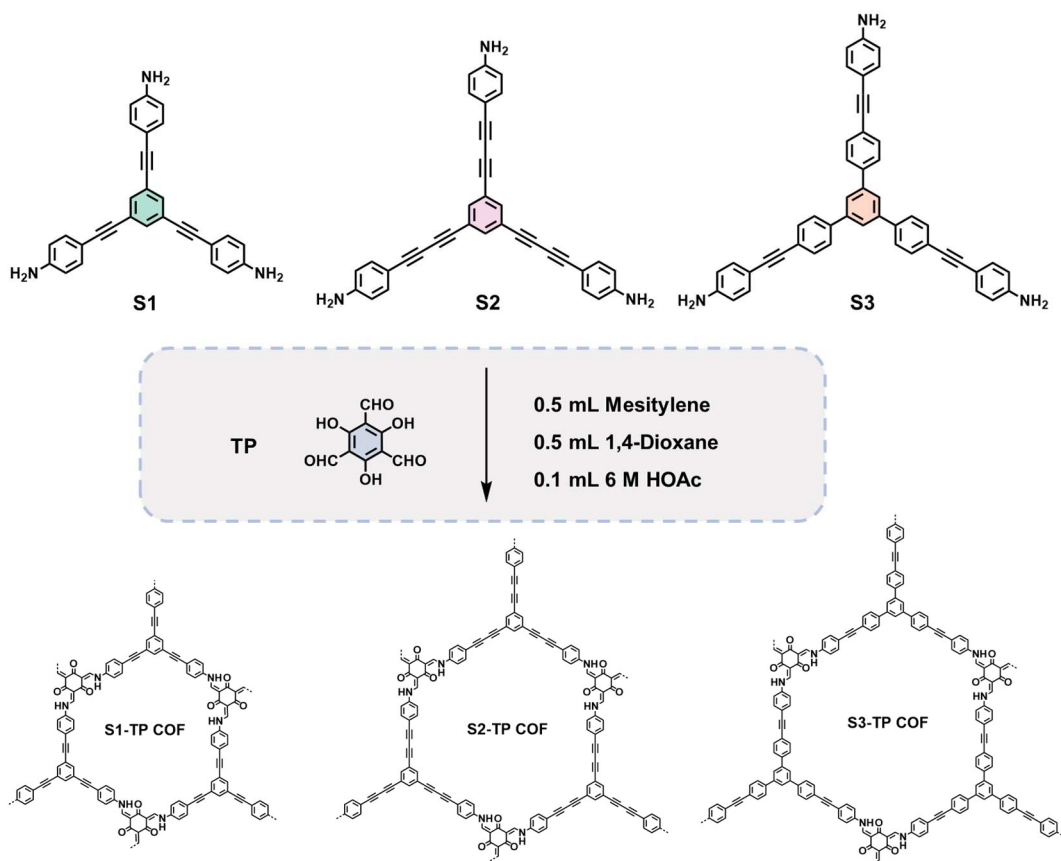


Figure S8. ^{13}C NMR spectrum of compound **S3** in $\text{DMSO-}d_6$.



Scheme S3. The synthetic scheme for **TP-COFs**.

Synthesis of TP-COFs

The synthesis was carried out according to the literature.^[S3, S5] **S1/S2/S3** (48 μmol) and **Tp** (10 mg, 48 μmol) were dispersed into a glass tube (8 \times 150 mm) charged with the solution of 0.50 mL mesitylene/0.50 mL of 1,4-dioxane/0.1 mL of 6 M aqueous acetic acid/13 μL aniline. The mixture was sonicated for 10 minutes to form a homogenous dispersion. The reaction mixture was allowed to stay static at 120 $^{\circ}\text{C}$ for 3 days. After cooling, the precipitate was collected by filtration and washed with DMF, THF, and subjected to Soxhlet extraction with THF for 3 days. The orange red powder was collected and dried at 120 $^{\circ}\text{C}$ under vacuum overnight to give **S1/S2/S3-TP COF** (yield > 78 %).

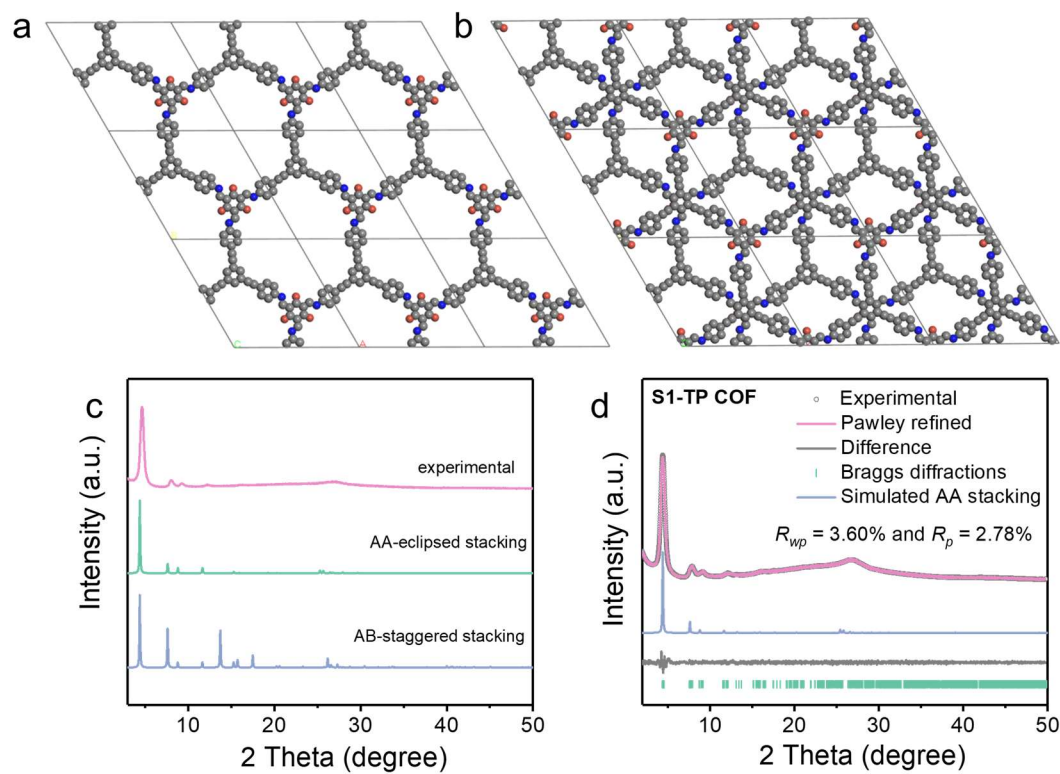


Figure S9. Simulated structure of **S1-TP COF** in (a) AA-eclipsed stacking and (b) AB-staggered stacking viewed along the *c* axis. (c) Simulated PXRD patterns of AA (green) and AB (blue) stacking model compared to the experimental pattern (pink) of **S1-TP COF**. (d) Experimental, simulated, and Pawley refined PXRD patterns of **S1-TP COF**.

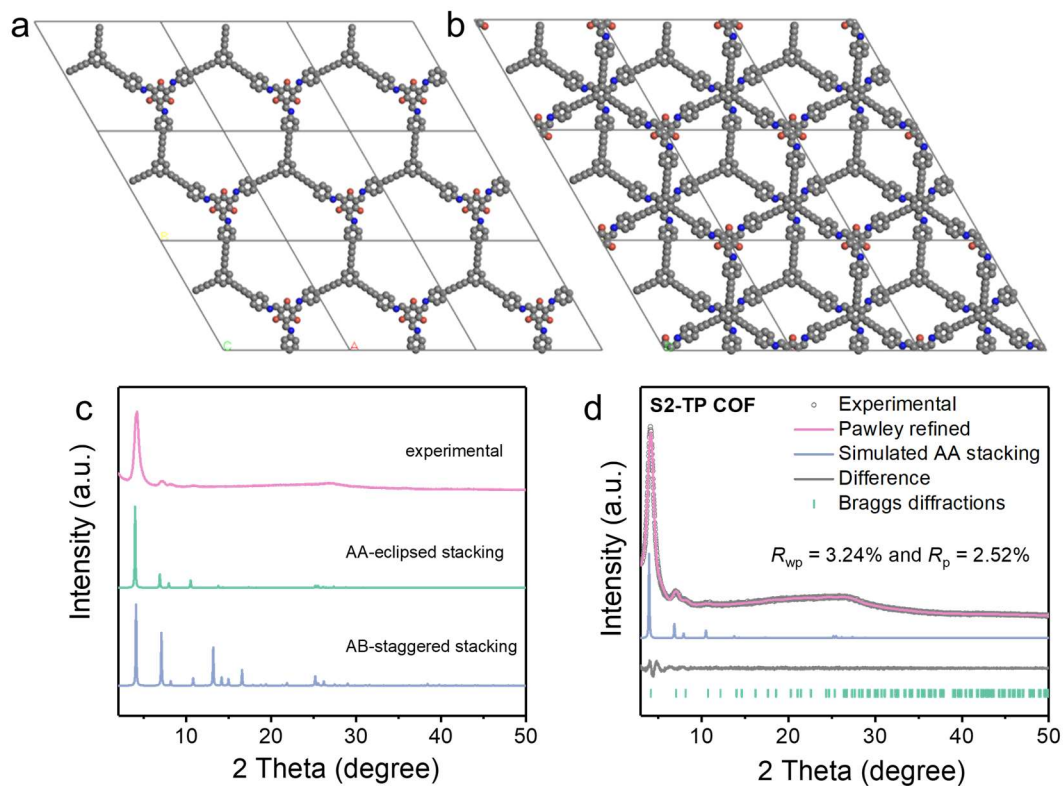


Figure S10. Simulated structure of **S2-TP COF** in (a) AA-eclipsed stacking and (b) AB-staggered stacking viewed along the *c* axis. (c) Simulated PXRD patterns of AA (green) and AB (blue) stacking model compared to the experimental pattern (pink) of **S2-TP COF**. (d) Experimental, simulated, and Pawley refined PXRD patterns of **S2-TP COF**.

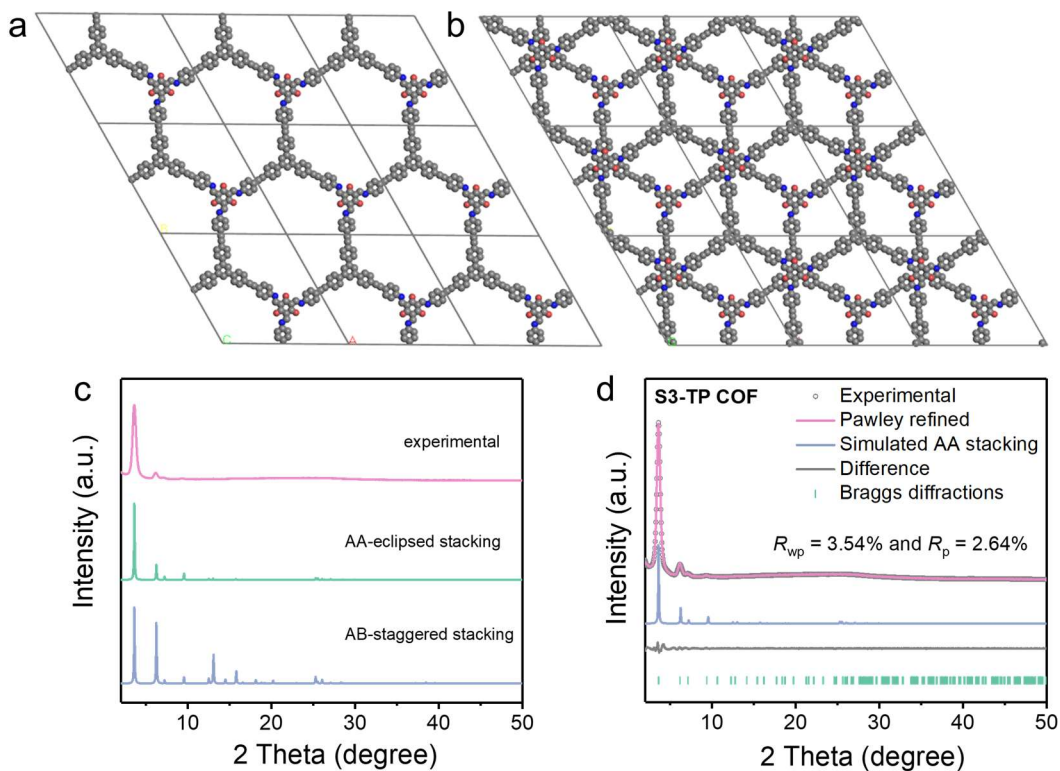


Figure S11. Simulated structure of **S3-TP COF** in (a) AA-eclipsed stacking and (b) AB-staggered stacking viewed along *c* axis. (c) Simulated PXRD patterns of AA (green) and AB (blue) stacking model compared to experimental pattern (pink) of **S3-TP COF**. (d) Experimental, simulated, and Pawley refined PXRD patterns of **S3-TP COF**.

Table S1. The unit cell structure of **TP-COFs**

COFs	Simulation structure parameters	Pawley refined unit cell parameters
S1-TP COF	AA stacking mode Hexagonal Space group symmetry <i>P6</i>	$a = b = 23.18 \text{ \AA}$, $c = 3.52 \text{ \AA}$ $\alpha = \beta = 90^\circ$, $\gamma = 120^\circ$ $R_{wp} = 3.60\%$ and $R_p = 2.78\%$
S2-TP COF	AA stacking mode Hexagonal Space group symmetry <i>P6</i>	$a = b = 25.10 \text{ \AA}$, $c = 3.34 \text{ \AA}$ $\alpha = \beta = 90^\circ$, $\gamma = 120^\circ$ $R_{wp} = 3.24\%$ and $R_p = 2.52\%$
S3-TP COF	AA stacking mode Hexagonal Space group symmetry <i>P6</i>	$a = b = 27.75 \text{ \AA}$, $c = 3.29 \text{ \AA}$ $\alpha = \beta = 90^\circ$, $\gamma = 120^\circ$ $R_{wp} = 3.54\%$ and $R_p = 2.64\%$

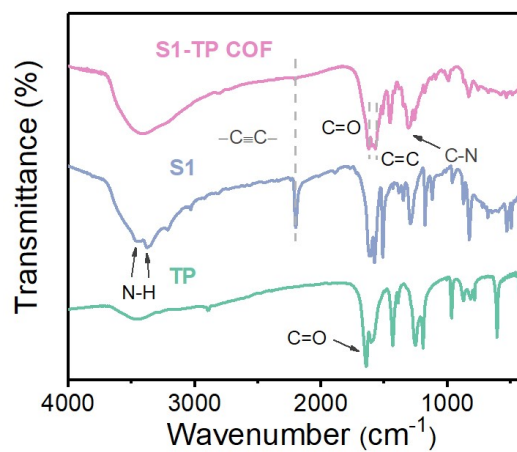


Figure S12. FT-IR spectra of S1-TP COF.

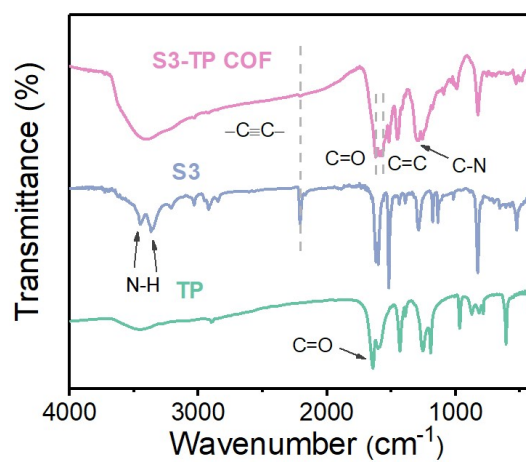


Figure S13. FT-IR spectra of S3-TP COF.

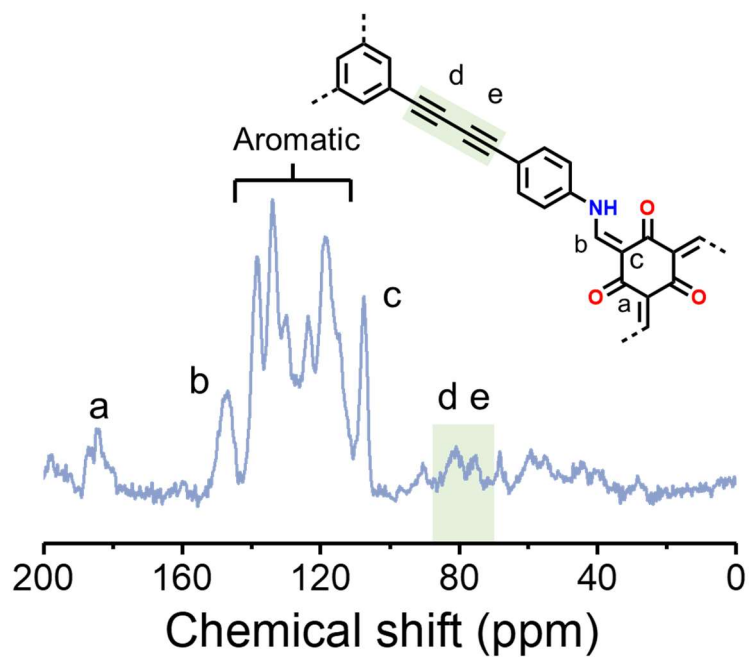


Figure S14. ^{13}C CP/MAS NMR spectroscopic analysis of S2-TP COF.

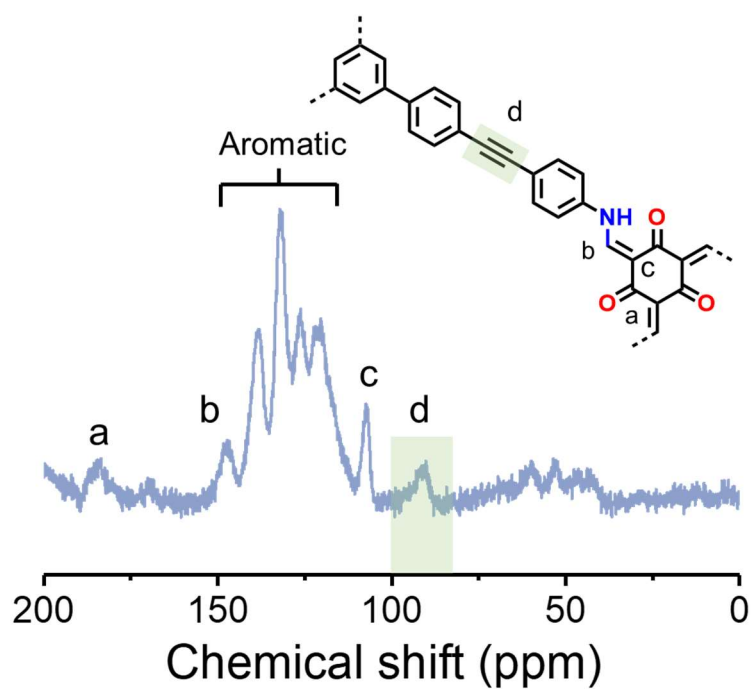


Figure S15. ^{13}C CP/MAS NMR spectroscopic analysis of S3-TP COF.

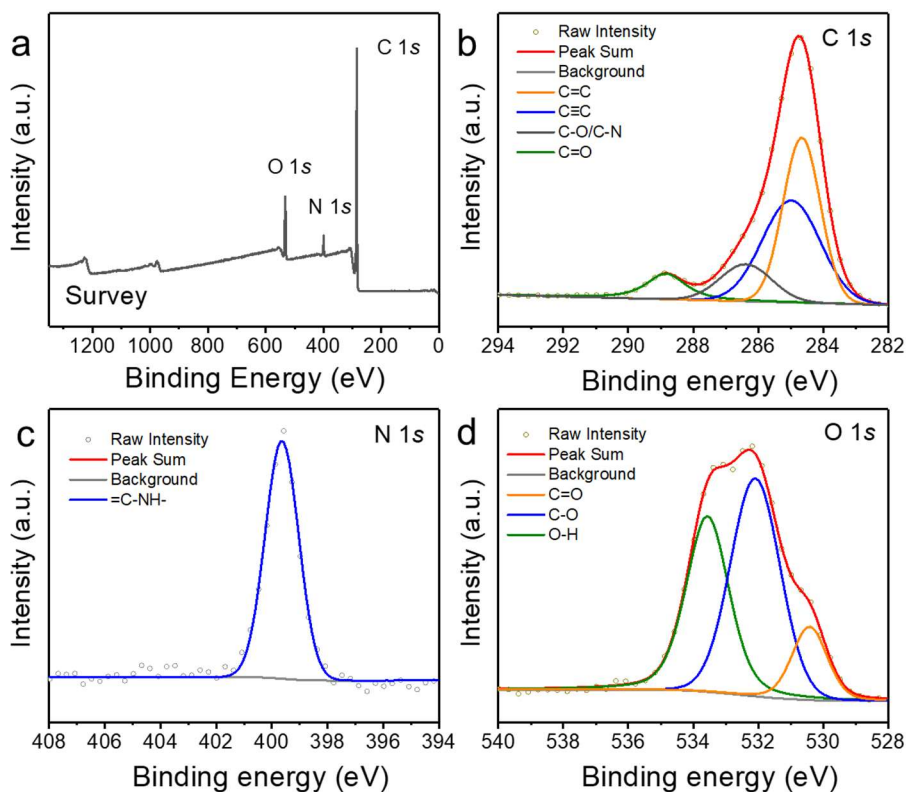


Figure S16. XPS spectra of S2-TP COF, (a) Survey scans, (b) C 1s, (c) N 1s, (d) O 1s peaks.

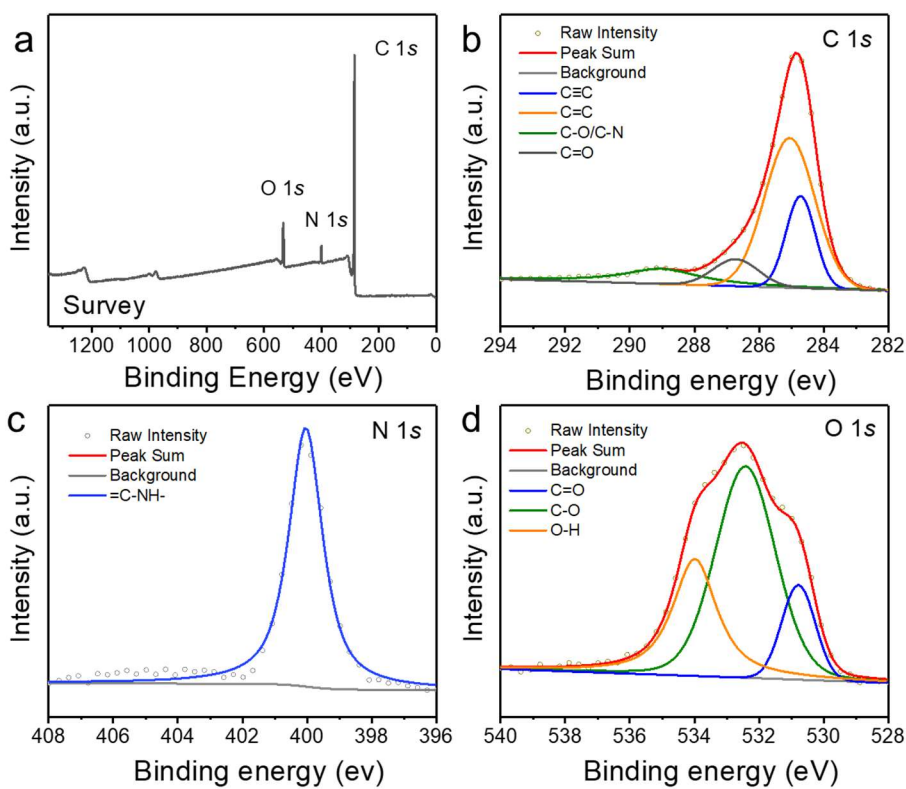


Figure S17. XPS spectra of S3-TP COF, (a) Survey scans, (b) C 1s, (c) N 1s, (d) O 1s peaks.

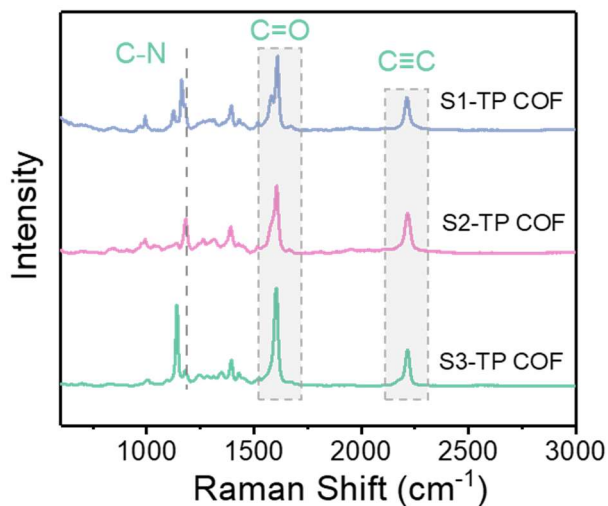


Figure S18. Raman spectra of TP-COFs.

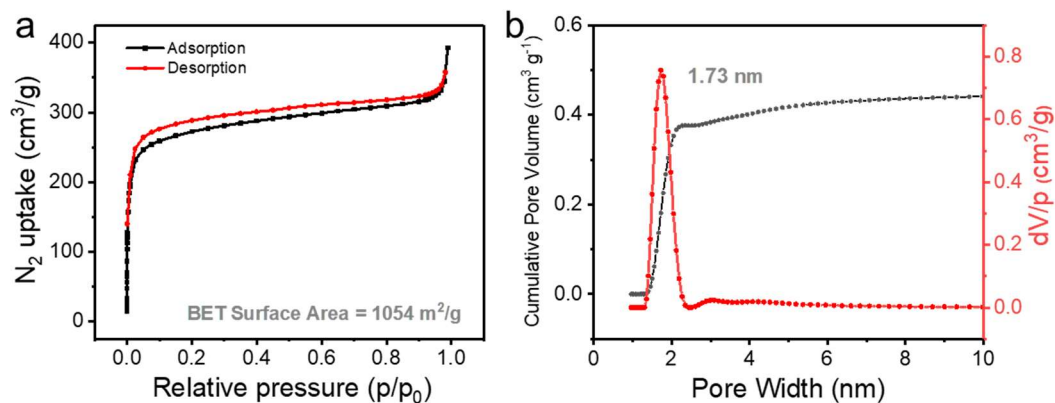


Figure S19. (a) N_2 sorption isotherms (type-I) and (b) pore size distribution profiles calculated by NLDFT of S1-TP COF.

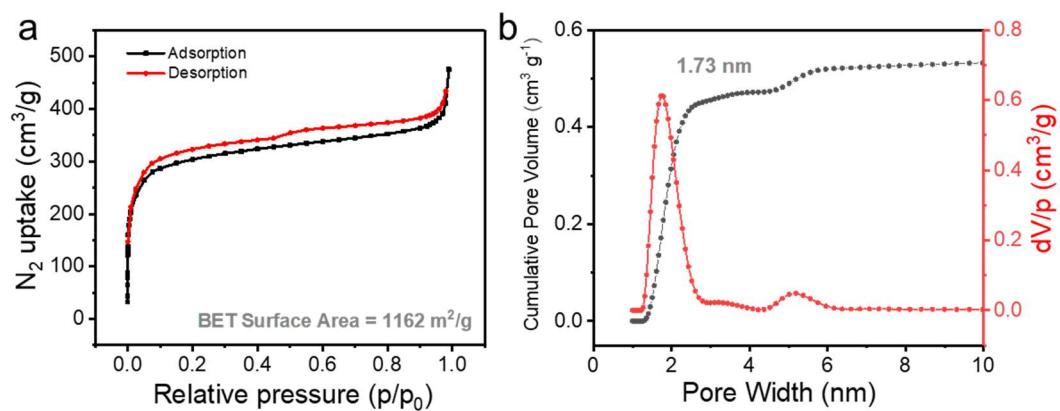


Figure S20. (a) N_2 sorption isotherms (type-I) and (b) pore size distribution profiles calculated by NLDFT of S2-TP COF.

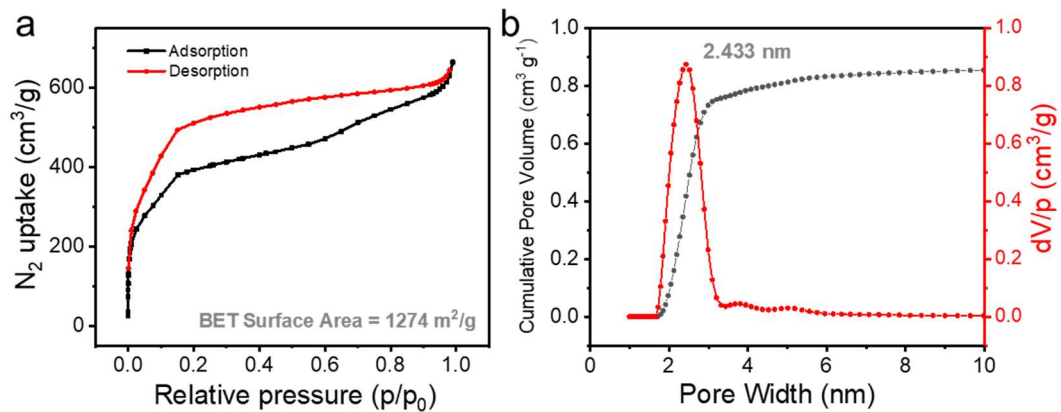


Figure S21. (a) N_2 sorption isotherms (type-IV) and (b) pore size distribution profiles calculated by NLDFT of S3-TP COF.

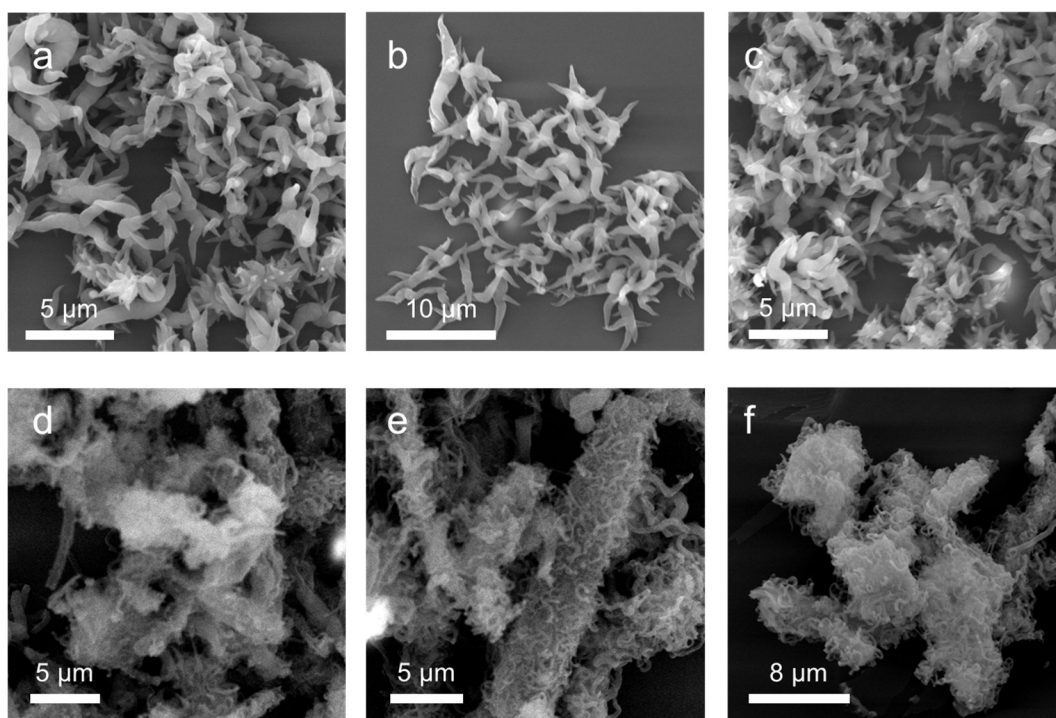


Figure S22. The SEM images of (a, b, c) S2-TP COF and (d, e, f) S3-TP COF.

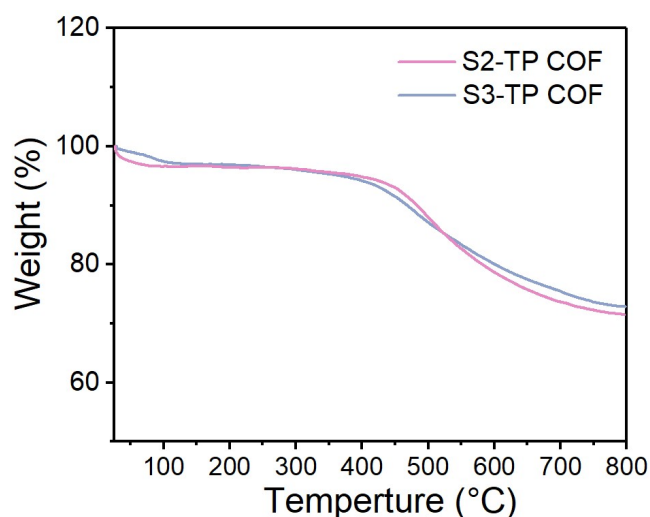


Figure S23. TGA curves of S2-TP COF (pink) and S3-TP COF (blue).

Thermogravimetric analysis. The thermal stability of the powder samples was evaluated by heating the activated samples from room temperature to 800 °C under a continuous flow of N₂ gas at the heating rate of 10 °C/minute. The TGA traces are typical of other reported COFs, exhibiting high thermal stability up to 400 °C.

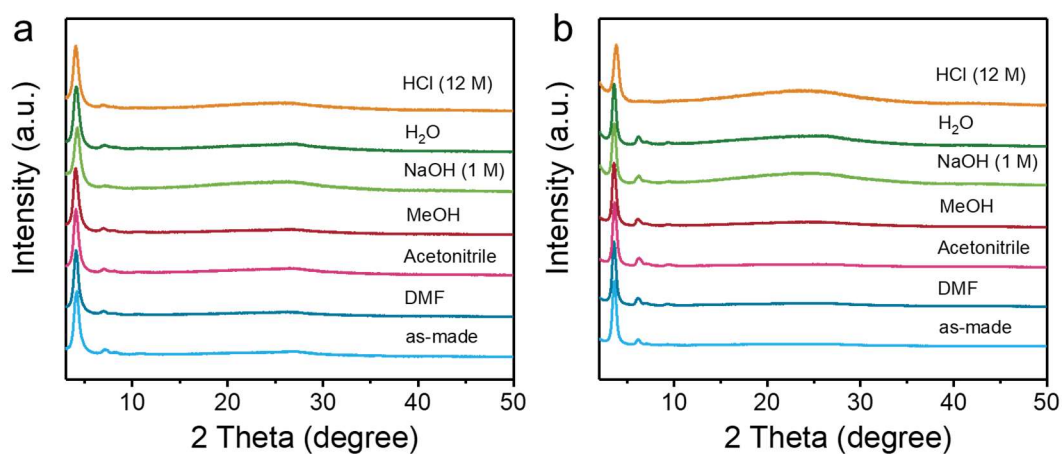


Figure S24. PXRD patterns of (a) S2-TP COF and (b) S3-TP COF immersed in various solutions for 3 days.

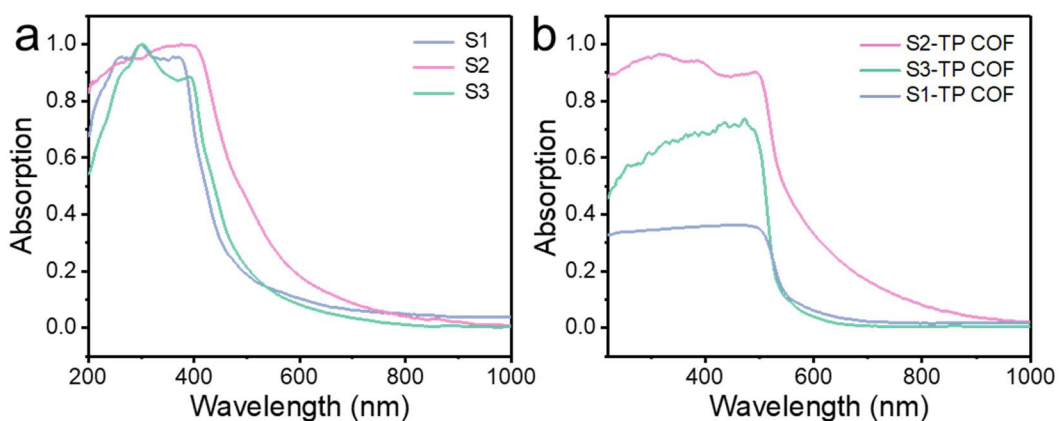


Figure S25. UV-Vis-NIR absorption spectra at room temperature of (a) monomers, and (b) TP-COFs.

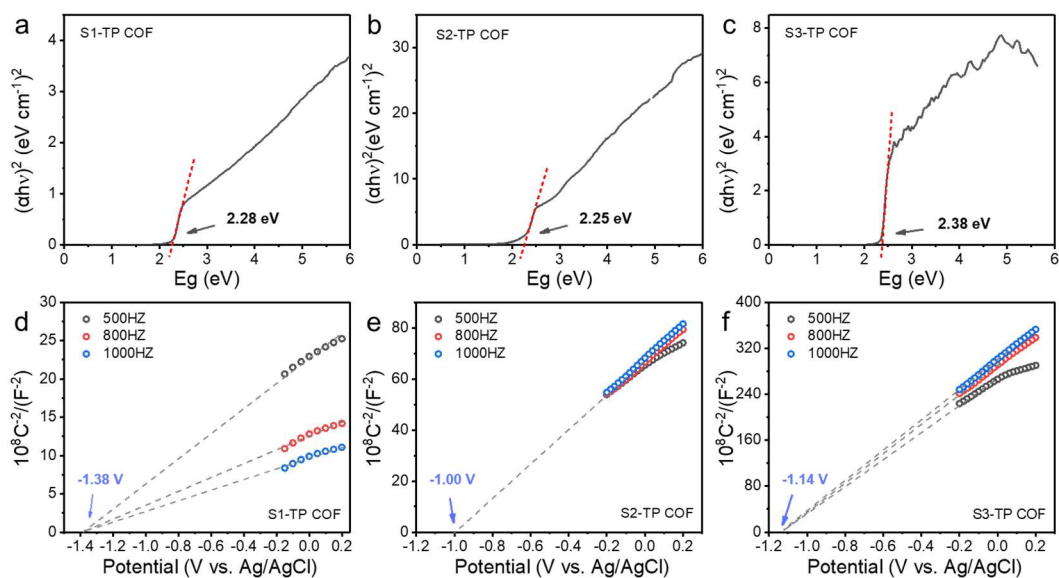


Figure S26. Tauc plots of **S1-TP COF** (a), **S2-TP COF** (b), and **S3-TP COF** (c). Mott-Schottky plots of **S1-TP COF** (d), **S2-TP COF** (e), and **S3-TP COF** (f) under different frequencies. Positive slopes of the Mott-Schottky plots signify these COFs to be *n*-type semiconductors.

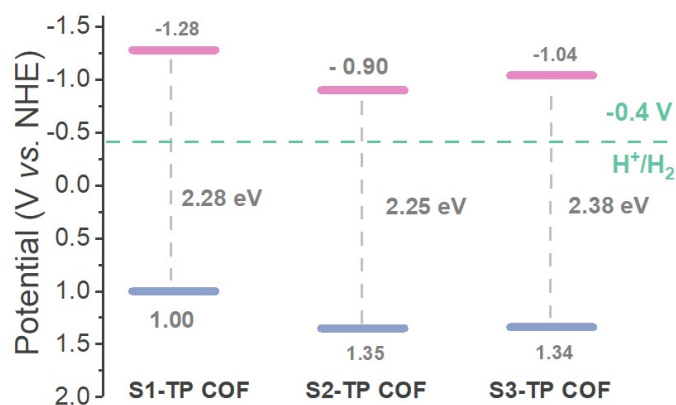


Figure S27. Band structure diagram of **S1-TP COF**, **S2-TP COF**, and **S3-TP COF** (note: the electrochemical potentials at pH = 6.8). In general, the CB edge position is more negative by about 0.1~0.3 V than the flat band potential for *n*-type semiconductors.

The flat band (V_{FB}) can be calculated from the x-intercept of the linear region of the M-S plots *via* Mott-Schottky equation:

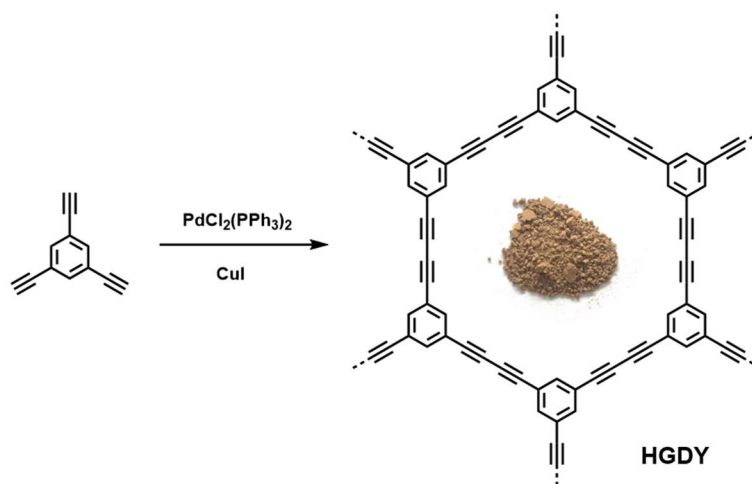
$$\frac{1}{C^2} = \frac{2}{\epsilon\epsilon_0 e N_D} \times \left(V - V_{FB} - \frac{k_B T}{e} \right)$$

where C refers to interfacial capacitance, ϵ and ϵ_0 are dielectric constant and vacuum dielectric constant, respectively, N_D is the donor density, V is the electrode potential, k_B is the Boltzmann constant, e is the elementary charge, and T is the absolute temperature.

Tauc plot (UV-Vis-NIR spectrum for calculation of bandgap): the above cutting line method applies to the direct bandgap of transmission spectrum that limits its large application. Tauc plot is mainly based on the formula proposed by Tauc, Davis and Mott *et al.*: $(\alpha h\nu)^{1/n} = B(h\nu - E_g)$, where α is absorption coefficient, h is Planck constant, ν is frequency, B is constant, E_g is the bandgap width of semiconductor, Exponential n is directly related to the type of semiconductor, direct bandgap $n = 1/2$, indirect bandgap $n = 2$.

Table S2. Elemental analysis results of **S2-TP COF** and **S3-TP COF** powder.

COFs		(C) %	(N) %	(H) %
S2-TP COF	Calcd.	73.76	5.73	4.13
	Found	73.03	6.65	4.80
	Calcd. formula	$(C_{45}H_{27}N_3O_3)(H_2O)_{4.5}$		
S3-TP COF	Calcd.	79.10	4.85	4.59
	Found	79.19	5.41	5.09
	Calcd. formula	$(C_{57}H_{33}N_3O_3)(H_2O)_{3.2}$		



Scheme S4. The synthetic scheme for **HGDY**.

Synthesis of HGDY

The synthesis was modified from a previous published protocol^[S6]. 1,3,5-Triethynylbenzene (150 mg, 1 mmol), CuI (11.4 mg, 0.06 eq.), $PdCl_2(PPh_3)_2$ (21.03 mg, 0.03 eq.) were loaded into a 25-mL Schlenk tube. The mixture was evacuated and backfilled with N_2 three times followed by addition of 5 mL triethylamine and 5 mL toluene under N_2 atmosphere to initiate the Sonogashira reaction. The reaction was maintained at 75 °C for 24 hours. Upon cooling to room temperature, the precipitate was collected by filtration and washed with DMF, DCM and subjected to Soxhlet extraction with THF for 3 days, resulting in the formation of the **HGDY** powder (yield: 91 %).

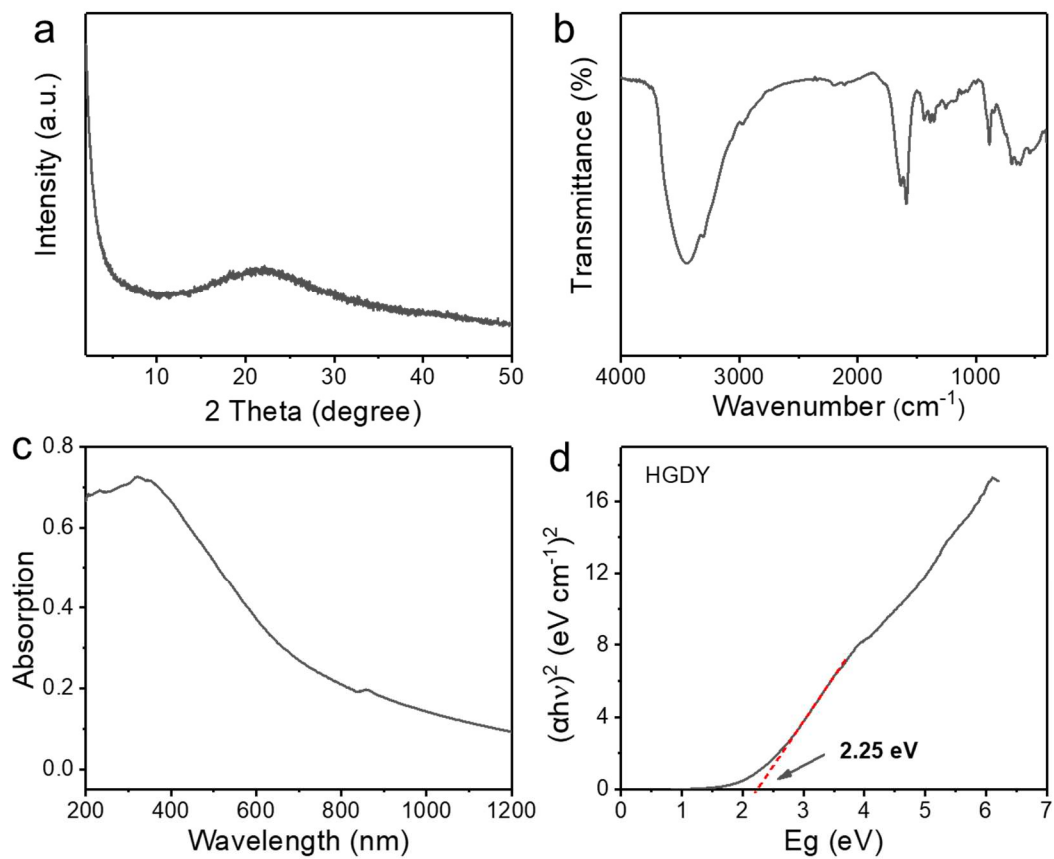


Figure S28. PXRD pattern (a), FT-IR spectrum (b), UV-Vis-NIR absorption spectrum at room temperature (c) and Tauc plot (d) of **HG DY**.

Photocatalytic hydrogen generation experiment



Figure S29. Water contact angles of ligands.



Figure S30. Water contact angles of COFs.



Figure S31. 0.5 M AA aqueous solution contact angles of COFs.

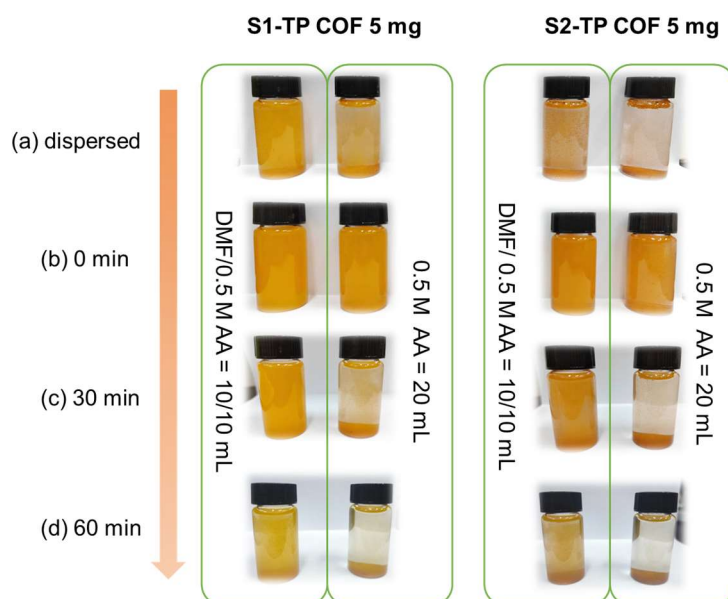


Figure S32. (a) The photos of COFs powder dispersed in different solutions. The photos of COFs powder ultrasonically dispersed in different solutions for 2 minutes and then allowed to stand still for (a) 0 minute; (b) 30 minutes and (c) 60 minutes.

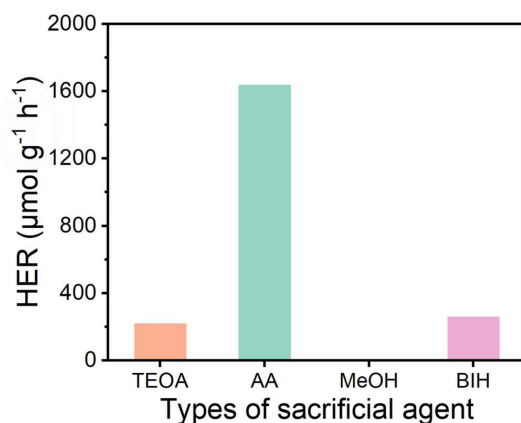


Figure S33. Photocatalytic H_2 evolution rates of **S2-TP COF** using different scavengers (Experimental conditions corresponding to **Table S3**).

Table S3. Photocatalytic H_2 evolution rates of **S2-TP COF** using different scavengers.

	S2-TP COF	Solvent	AA aqueous solution (0.5 M)	H_2PtCl_6 aqueous solution (5 mg/mL)	HER ($\mu\text{mol/g/h}$)
1	5 mg	DMF/ H_2O (4.5/4.5 mL)	TEOA (1 mL)	3% (30 μL)	220.8
2	5 mg	DMF/ H_2O (4.5/4.5 mL)	AA (20 mg)	3% (30 μL)	1637.3
3	5 mg	H_2O (1 mL)	MeOH (9 mL)	3% (30 μL)	0.85
4	5 mg	DMF/ H_2O (4.5/4.5 mL)	BIH (10 mg)	3% (30 μL)	261.7

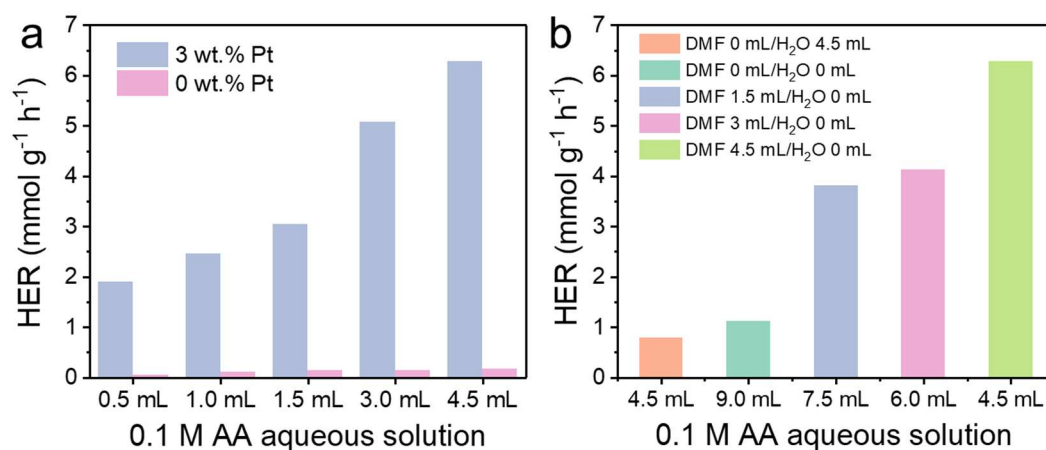


Figure S34. (a) Photocatalytic H_2 evolution rates of **S2-TP COF** with different volumes of 0.1 M AA aqueous solution (Experimental conditions listed in **Table S4**). (b) Photocatalytic H_2 evolution rates of **S2-TP COF** with different volumes of DMF (Experimental conditions listed in **Table S5**).

Table S4. Photocatalytic H₂ evolution rates of **S2-TP COF** with different volumes of 0.1 M AA aqueous solution.

	S2-TP COF	Solvent	AA aqueous solution (0.1 M)	H ₂ PtCl ₆ aqueous solution (5 mg/mL)	HER (μmol/g/h)
1	5 mg	DMF/H ₂ O (4.5/4.0 mL)	0.5 mL	3% (30 μL)	1902.4
2	5 mg	DMF/H ₂ O (4.5/3.5 mL)	1.0 mL	3% (30 μL)	2456.2
3	5 mg	DMF/H ₂ O (4.5/3.0 mL)	1.5 mL	3% (30 μL)	3042.8
4	5 mg	DMF/H ₂ O (4.5/1.5 mL)	3.0 mL	3% (30 μL)	5081.9
5	5 mg	DMF/H ₂ O (4.5/0 mL)	4.5 mL	3% (30 μL)	6286.6
6	5 mg	DMF/H ₂ O (4.5/3.5 mL)	1.0 mL	0%	113.7
7	5 mg	DMF/H ₂ O (4.5/3.0 mL)	1.5 mL	0%	147.5
8	5 mg	DMF/H ₂ O (4.5/1.5 mL)	3.0 mL	0%	142.8
9	5 mg	DMF/H ₂ O (4.5/0 mL)	4.5 mL	0%	166.2

Table S5. Photocatalytic H₂ evolution rates of **S2-TP COF** with different volumes of DMF.

	S2-TP COF	Solvent	AA aqueous solution (0.1 M)	H ₂ PtCl ₆ aqueous solution (5 mg/mL)	HER (μmol/g/h)
1	5 mg	DMF/H ₂ O (0/4.5 mL)	4.5 mL	3% (30 μL)	790.1
2	5 mg	DMF/H ₂ O (0/0 mL)	9.0 mL	3% (30 μL)	1114.7
3	5 mg	DMF/H ₂ O (1.5/0 mL)	7.5 mL	3% (30 μL)	3817.5
4	5 mg	DMF/H ₂ O (3.0/0 mL)	6.0 mL	3% (30 μL)	4129.1
5	5 mg	DMF/H ₂ O (4.5/0 mL)	4.5 mL	3% (30 μL)	6286.6

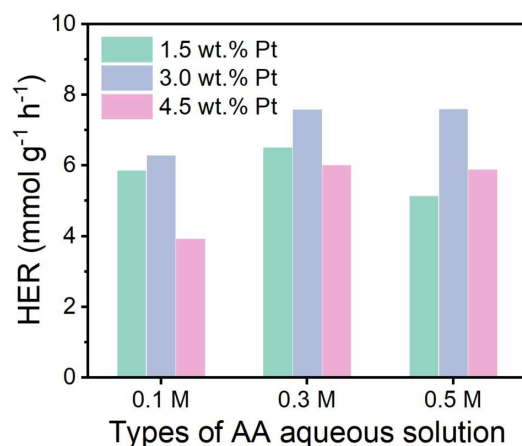


Figure S35. Photocatalytic H₂ evolution rates of S2-TP COF with different Pt loading amounts (Experimental conditions listed in Table S6).

Table S6. Photocatalytic H₂ evolution rates of S2-TP COF with different Pt loading amounts.

	S2-TP COF	Solvent (DMF)	AA aqueous solution (0.1 M)	H ₂ PtCl ₆ aqueous solution (5 mg/mL)	HER (μmol/g/h)
1	5 mg	4.5 mL	4.5 mL	1.5% (15 μL)	5865.3
2	5 mg	4.5 mL	4.5 mL	3.0% (30 μL)	6286.6
3	5 mg	4.5 mL	4.5 mL	4.5% (45 μL)	3921.3
	S2-TP COF	Solvent (DMF)	AA aqueous solution (0.3 M)	H ₂ PtCl ₆ aqueous solution (5 mg/mL)	HER (μmol/g/h)
4	5 mg	4.5 mL	4.5 mL	1.5% (15 μL)	6511.2
5	5 mg	4.5 mL	4.5 mL	3.0% (30 μL)	7575.7
6	5 mg	4.5 mL	4.5 mL	4.5% (45 μL)	6009.9
	S2-TP COF	Solvent (DMF)	AA aqueous solution (0.5 M)	H ₂ PtCl ₆ aqueous solution (5 mg/mL)	HER (μmol/g/h)
7	5 mg	4.5 mL	4.5 mL	1.5% (15 μL)	5139.7
8	5 mg	4.5 mL	4.5 mL	3.0% (30 μL)	7594.5
9	5 mg	4.5 mL	4.5 mL	4.5% (45 μL)	5885.4

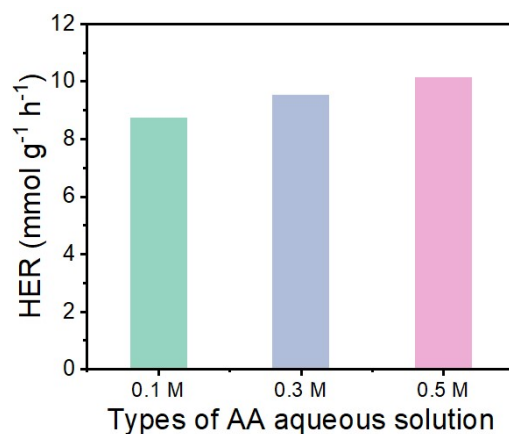


Figure S36. Photocatalytic H₂ evolution rates of **S2-TP COF** with 20 mL mixed solvent. (Experimental conditions listed in **Table S7**).

Table S7. Photocatalytic H₂ evolution rates of **S2-TP COF** with 20 mL mixed solvent.

	S2-TP COF	Solvent (DMF)	AA aqueous solution (0.1 M)	H ₂ PtCl ₆ aqueous solution (5 mg/mL)	HER (μmol/g/h)
1	5 mg	10 mL	10 mL	3.0% (30 μL)	8751.7
2	5 mg	10 mL	10 mL	3.0% (30 μL)	9538.5
3	5 mg	10 mL	10 mL	3.0% (30 μL)	10158.1
4	5 mg	0	20 mL	3.0% (30 μL)	3264.9

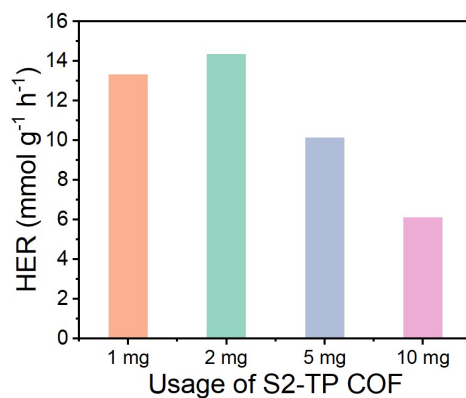


Figure S37. Photocatalytic H₂ evolution rates with different amounts of **S2-TP COF**.

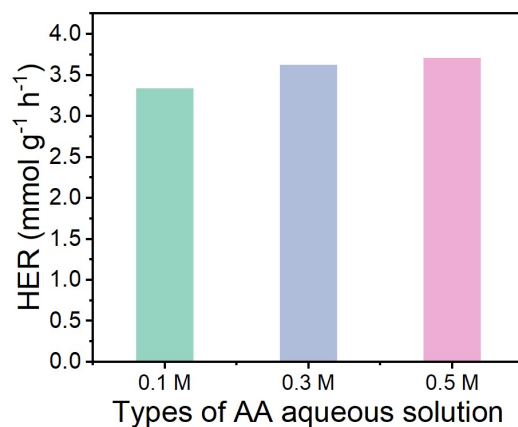


Figure S38. Photocatalytic H₂ evolution rates of **S1-TP COF**. (Experimental conditions listed in **Table S8**).

Table S8. Photocatalytic H₂ evolution rates of **S1-TP COF**.

	S1-TP COF	Solvent (DMF)	AA aqueous solution (0.1 M)	H ₂ PtCl ₆ aqueous solution (5 mg/mL)	HER (μmol/g/h)
1	5 mg	10 mL	10 mL	3.0% (30 μL)	3338.6
	S1-TP COF	Solvent (DMF)	AA aqueous solution (0.3 M)	H ₂ PtCl ₆ aqueous solution (5 mg/mL)	HER (μmol/g/h)
2	5 mg	10 mL	10 mL	3.0% (30 μL)	3624.8
	S1-TP COF	Solvent (DMF)	AA aqueous solution (0.5 M)	H ₂ PtCl ₆ aqueous solution (5 mg/mL)	HER (μmol/g/h)
3	5 mg	10 mL	10 mL	3.0% (30 μL)	3708.9
4	5 mg	0 mL	20 mL	3.0% (30 μL)	1602.9

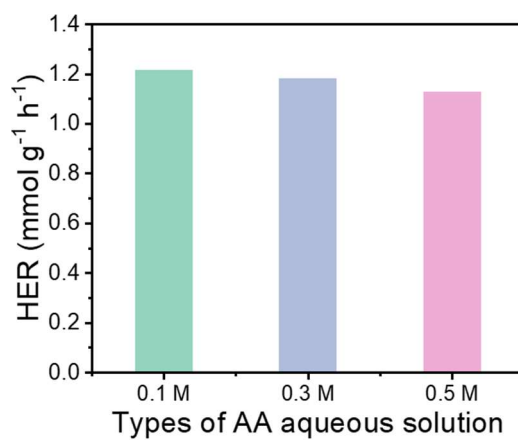
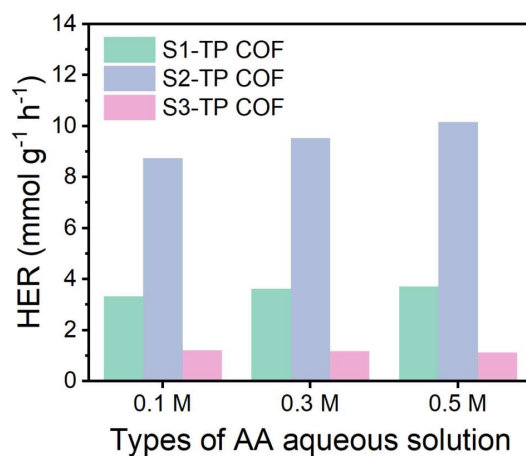


Figure S39. Photocatalytic H₂ evolution rates of **S3-TP COF**. (Experimental conditions listed in **Table S9**).

Table S9. Photocatalytic H₂ evolution rates of **S3-TP COF**.

	S3-TP COF	Solvent (DMF)	AA aqueous solution (0.1 M)	H ₂ PtCl ₆ aqueous solution (5 mg/mL)	HER (μmol/g/h)
1	5 mg	10 mL	10 mL	3.0% (30 μL)	1214.6
	S3-TP COF	Solvent (DMF)	AA aqueous solution (0.3 M)	H ₂ PtCl ₆ aqueous solution (5 mg/mL)	HER (μmol/g/h)
2	5 mg	10 mL	10 mL	3.0% (30 μL)	1182.6
	S3-TP COF	Solvent (DMF)	AA aqueous solution (0.5 M)	H ₂ PtCl ₆ aqueous solution (5 mg/mL)	HER (μmol/g/h)
3	5 mg	10 mL	10 mL	3.0% (30 μL)	1128.1
4	5 mg	0 mL	20 mL	3.0% (30 μL)	231.7

**Figure S40.** Comparison of photocatalytic H₂ evolution rates for **TP-COFs** in AA aqueous solution of different concentrations (Experimental conditions: 5 mg photocatalyst, 3 wt.% Pt as cocatalyst, 10/10 mL DMF/AA aqueous solution).

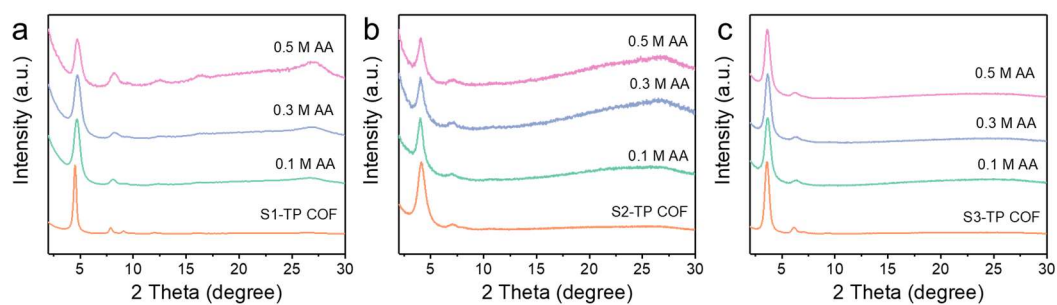


Figure S41. PXRD patterns of (a) S1-TP COF, (b) S2-TP COF, and (c) S3-TP COF powder before and after photocatalysis (Experimental conditions: 5 mg photocatalyst, 3 wt.% Pt as cocatalyst, 10/10 mL DMF/AA aqueous solution).

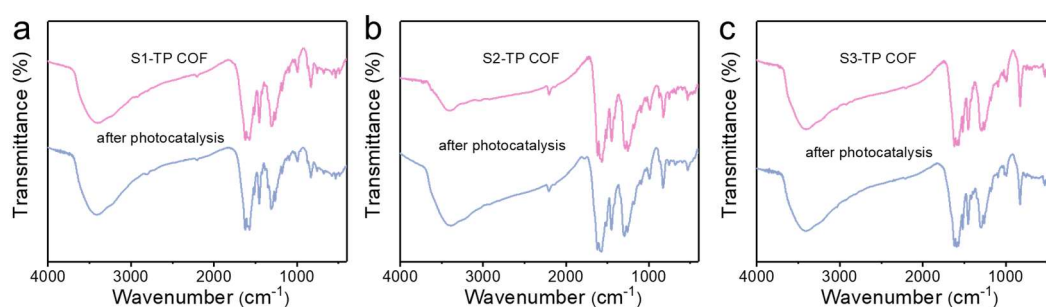


Figure S42. FT-IR spectra of TP-COFs powder before and after photocatalysis (Experimental conditions: 5 mg photocatalyst, 3 wt.% Pt as a cocatalyst, 10/10 mL DMF/0.5 M AA aqueous solution).

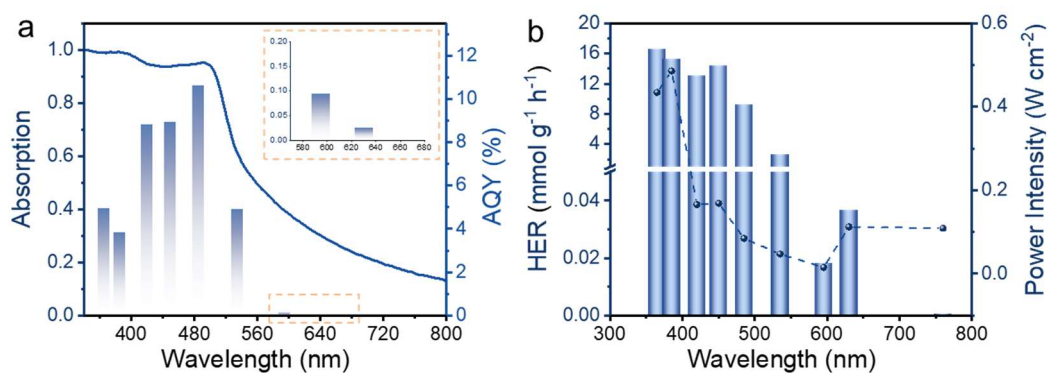


Figure S43. (a) AQY of S2-TP COF with 3 wt.% Pt at nine different incident light wavelengths for photocatalytic H₂ evolution. (b) Corresponding photocatalytic H₂ evolution rates and power density for different wavelengths.

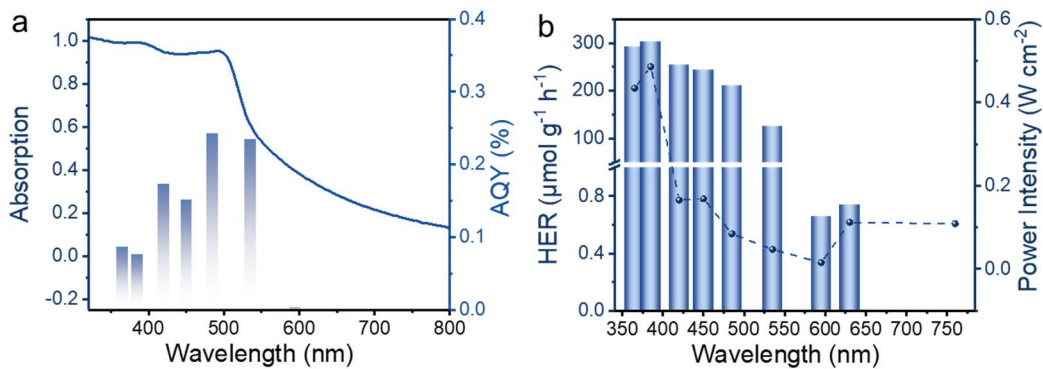


Figure S44. (a) AQY of S2-TP COF with 0 wt.% Pt at nine different incident light wavelengths for photocatalytic H₂ evolution. (b) Corresponding photocatalytic H₂ evolution rates and power density for different wavelengths.

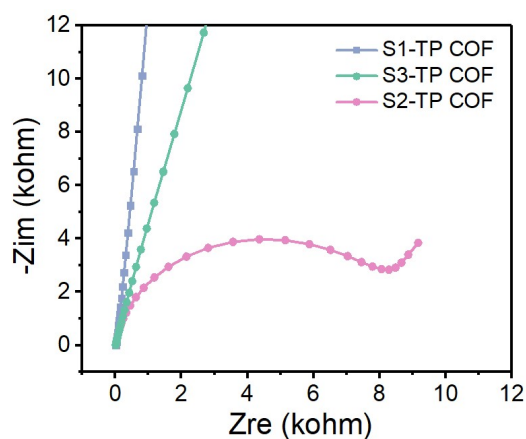


Figure S45. Nyquist plots/ EIS spectra without light irradiation of TP-COFs.

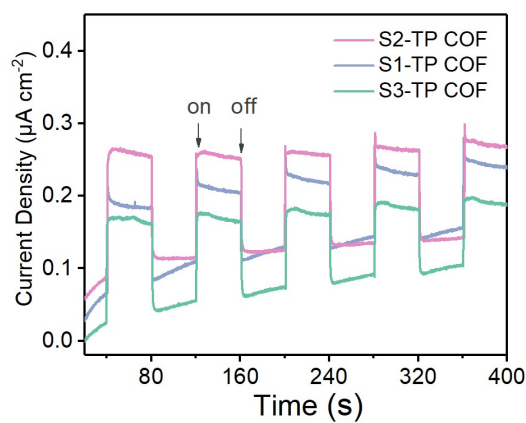


Figure S46. Photocurrent response plots of TP-COFs.

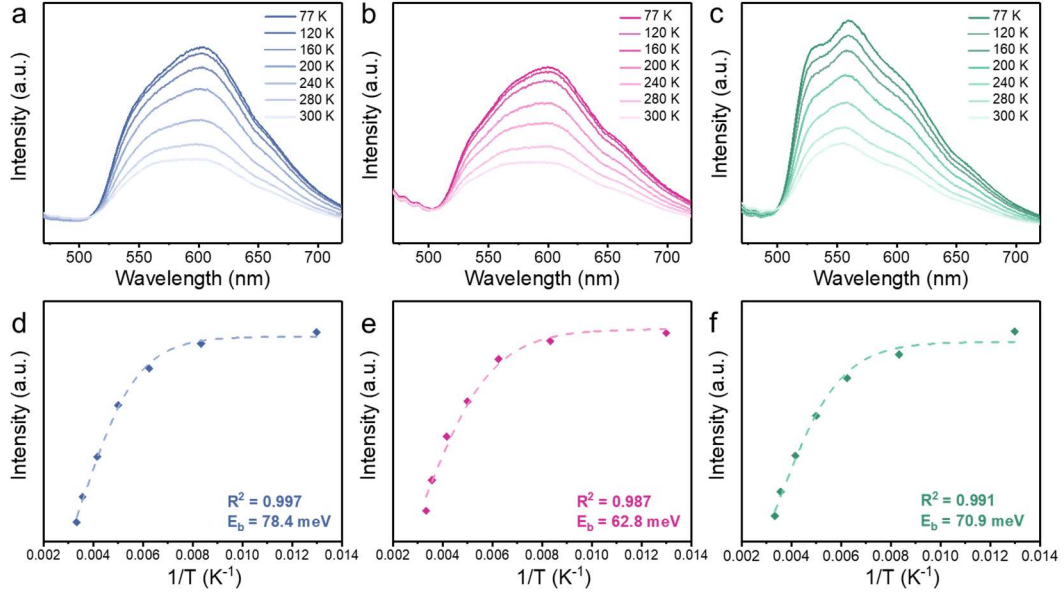


Figure S47. Exciton binding energies measurement. Temperature-dependent PL spectra from 77 to 300 K under the excitation wavelength of 370 nm; Integrated PL intensity as a function of temperature and the fitted exciton binding energy of **S1-TP COF** (a, d; blue), **S2-TP COF** (b, e; pink), and **S3-TP COF** (c, f; green).

The exciton binding energy could be fitted with the Arrhenius equation,

$$I(T) = \frac{I_0}{1 + Ae^{-E_b/k_B T}}$$

where I_0 is PL intensity at 0 K, A is the proportional constant, k_B is the Boltzmann constant ($8.62 \times 10^{-2} \text{ meV K}^{-1}$), and E_b is the binding energy.^[S7, S8]

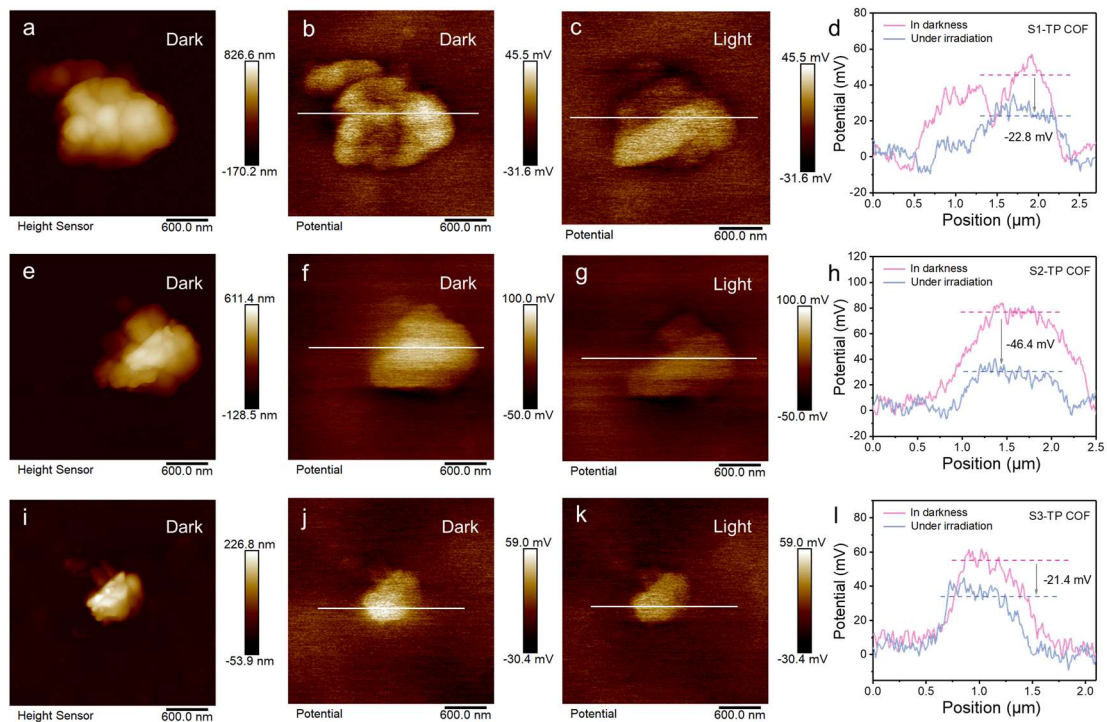


Figure S48. (a, e, i) KPFM surface topography mapping, surface potential distribution images of TP-COFs (b, f, g) in darkness and (c, g, k) under UV-light irradiation, (d, h, l) as well as the corresponding surface potential difference of the cross-section of TP-COFs before and after photoirradiation.

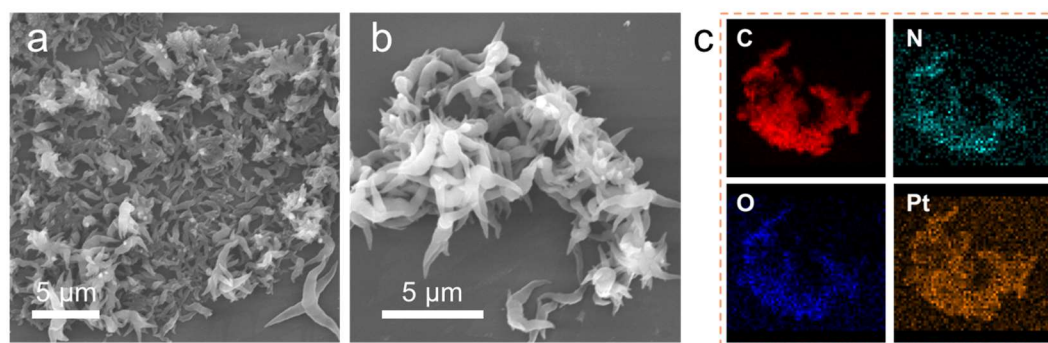


Figure S49. (a, b) The SEM images and (c) EDS elemental mappings of S2-TP COF after photocatalysis. (Experimental conditions: 5 mg photocatalyst, 3 wt.% Pt as cocatalyst, 10/10 mL DMF/0.5 M AA aqueous solution).

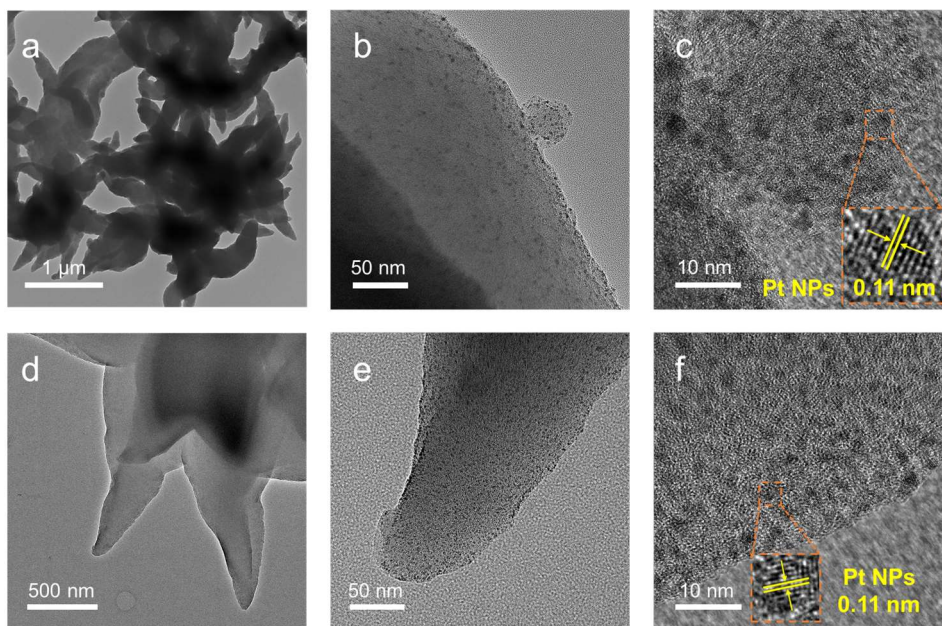


Figure S50. The TEM images of **S2-TP COF** after photocatalysis. (Experimental conditions: 5 mg photocatalyst, 3 wt.% Pt as a cocatalyst, 10/10 mL DMF/0.5 M AA aqueous solution).

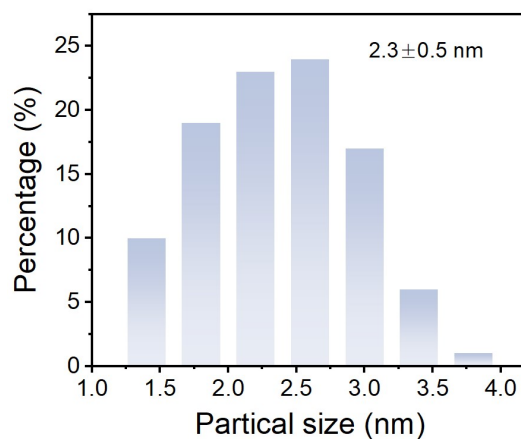


Figure S51. The Pt nanoparticle size distribution of **S2-TP COF** after photocatalysis calculated from the TEM images in Figure S50.

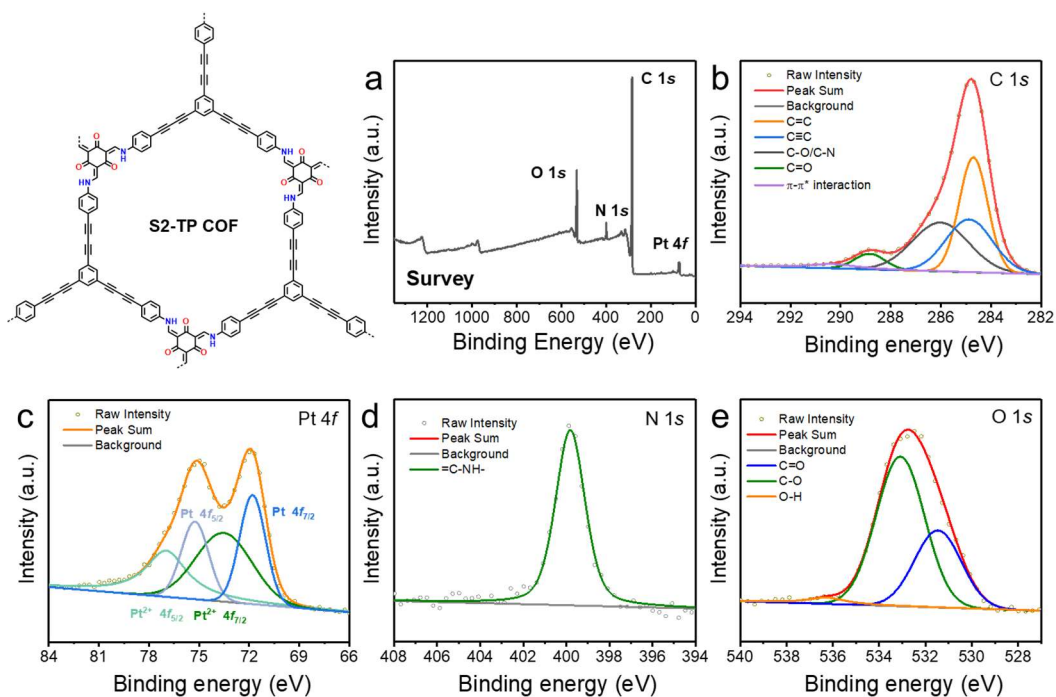


Figure S52. XPS spectra of S2-TP COF powder after photocatalysis, (a) Survey scans, (b) C 1s, (c) Pt 4f, (d) N 1s, (e) O 1s peaks. (Experimental conditions: 5 mg photocatalyst, 3 wt.% Pt as cocatalyst, 10/10 mL DMF/0.5 M AA aqueous solution).

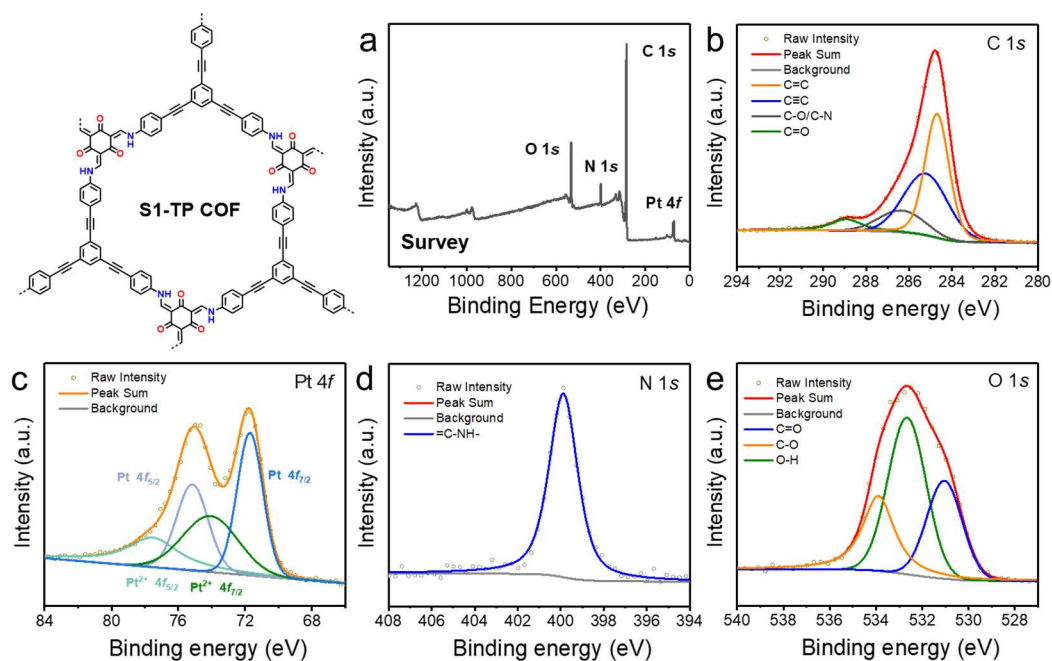


Figure S53. XPS spectra of S1-TP COF powder after photocatalysis, (a) Survey scans, (b) C 1s, (c) Pt 4f, (d) N 1s, (e) O 1s peaks. (Experimental conditions: 5 mg photocatalyst, 3 wt.% Pt as cocatalyst, 10/10 mL DMF/0.5 M AA aqueous solution).

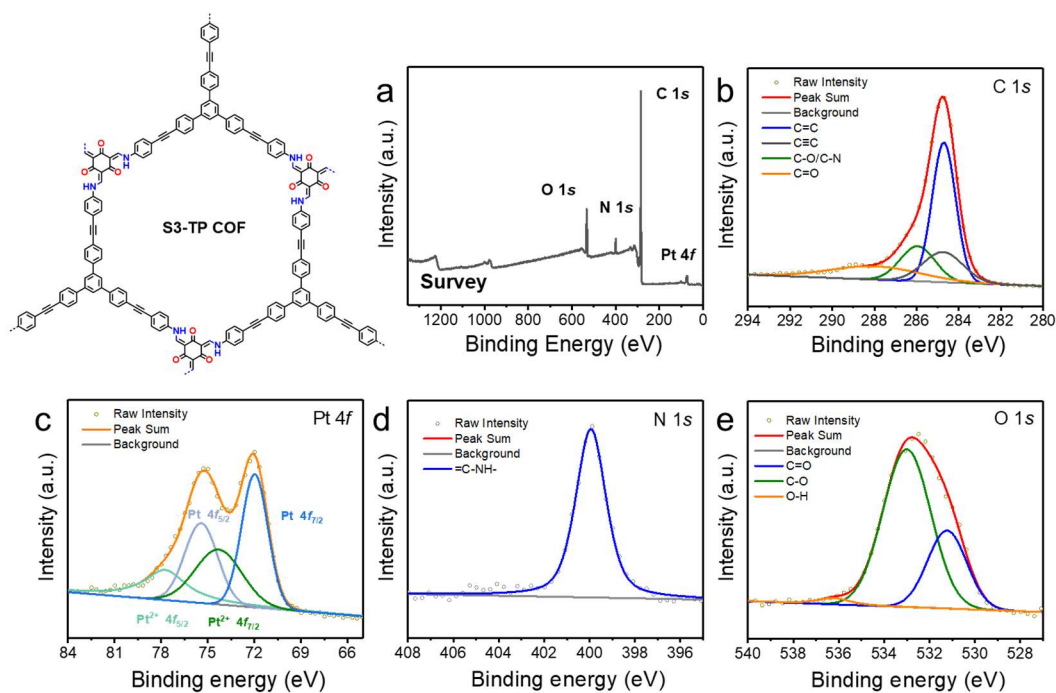


Figure S54. XPS spectra of **S3-TP COF** powder after photocatalysis, (a) Survey scans, (b) C 1s, (c) Pt 4f, (d) N 1s, (e) O 1s peaks. (Experimental conditions: 5 mg photocatalyst, 3 wt.% Pt as cocatalyst, 10/10 mL DMF/0.5 M AA aqueous solution).

Table S10. ICP-AES results of **TP-COFs** after photocatalysis (Experimental conditions: 5 mg photocatalyst, 3 wt.% Pt as a cocatalyst, 10/10 mL DMF/0.5 M AA aqueous solution).

Sample	Pt content (wt.%)
S1-TP COF	0.4163%
S2-TP COF	0.2893%
S3-TP COF	0.2874%

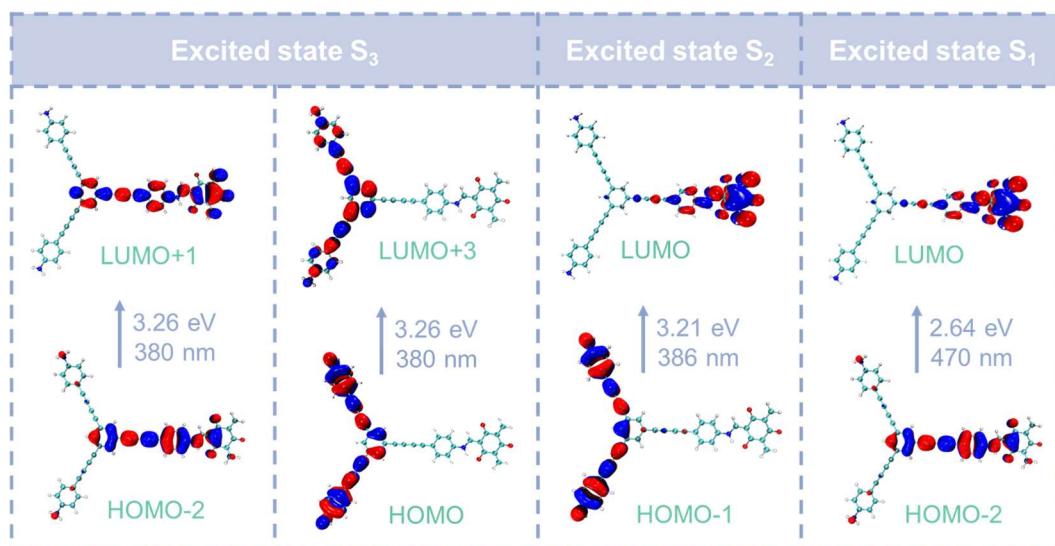


Figure S55. The TD-DFT calculated electronic transitions of S2-TP COF.

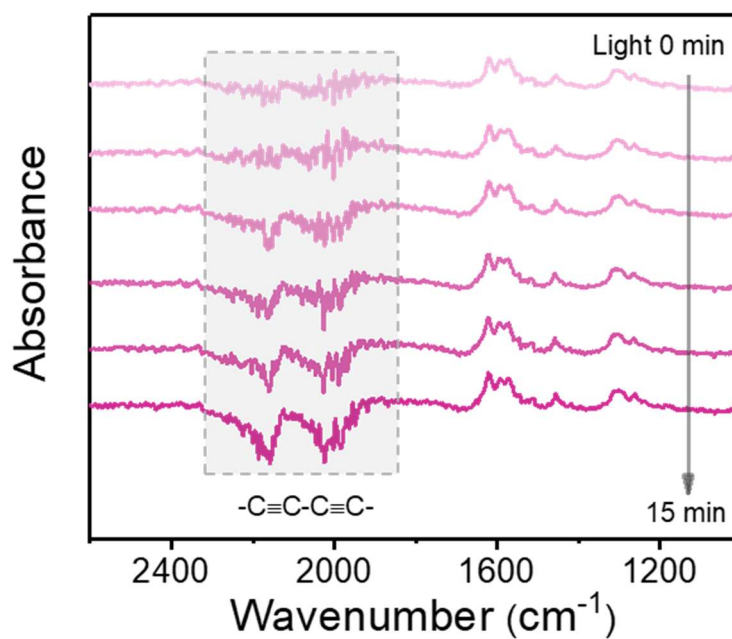


Figure S56. *In situ* IR spectra of S2-TP COF in pure H₂O with Pt salt under light irradiation.

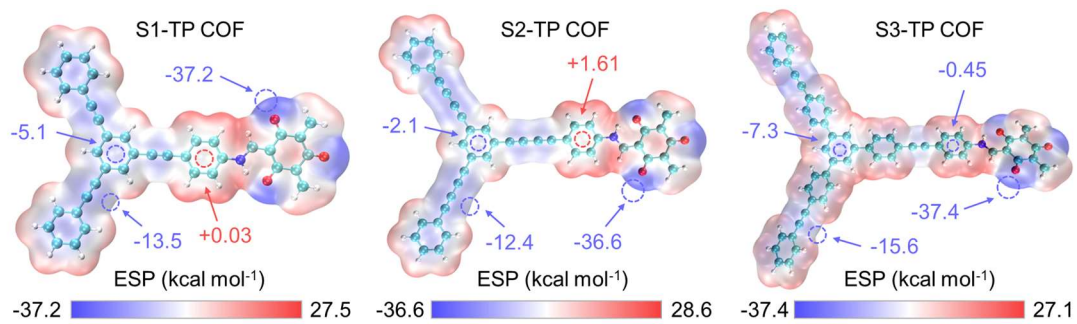


Figure S57. Electrostatic potential map of TP-COFs models (negative and positive regions indicated in blue and red respectively).

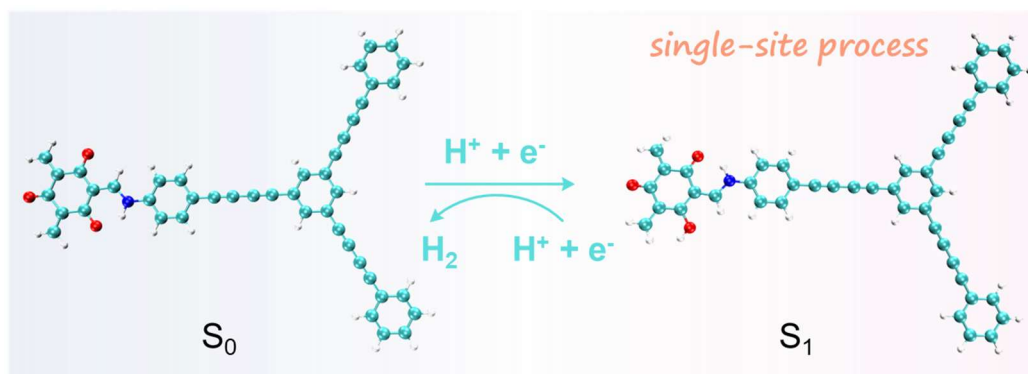


Figure S58. Proposed photocatalytic H₂ evolution processes on S2-TP COF (site 1).

References

- S1. T. Lu and F. Chen, Multiwfn: A multifunctional wavefunction analyzer, *J. Comput. Chem.* 2012, **33**, 580.
- S2. W. Humphrey, A. Dalke and K. Schulten, VMD: Visual molecular dynamics, *J. Mol. Graphics*, 1996, **14**, 33.
- S3. Z. Lin, Y.-H. Zhong, L. Zhong, X. Ye, L.-H. Chung, X. Hu, Z. Xu, L. Yu, and J. He, Minimalist Design for Solar Energy Conversion: Revamping the π -Grid of an Organic Framework into Open-Shell Superabsorbers. *JACS Au*, 2023, **3**, 1711–1722.
- S4. L. Su, J. Dong, L. Liu, M. Sun, R. Qiu, Y. Zhou, and S.-F. Yin, Copper Catalysis for Selective Heterocoupling of Terminal Alkynes, *J. Am. Chem. Soc.* 2016, **138**, 12348–12351.
- S5. X. Hu, Z. Lin, S. Wang, G. Zhang, S. Lin, T. Huang, R. Chen, L.-H. Chung, J. He, Highly Crystalline Flower-Like Covalent-Organic Frameworks Enable Highly Stable Zinc Metal Anodes. *ACS Appl. Energy Mater.*, 2022, **5**, 3715-3723.
- S6. P. Zhao, H. Jiang, H. Shen, S. Yang, R. Gao, Y. Guo, Q. Zhang and H. Zhang, Construction of Low-Coordination Cu–C₂ Single-Atoms Electrocatalyst Facilitating the Efficient Electrochemical CO₂ Reduction to Methane, *Angew. Chem. Int. Ed.*, 2023, **62**, e202314121.
- S7. G. Fu, D. Yang, S. Xu, S. Li, Y. Zhao, H. Yang, D. Wu, P. S. Petkov, Z.-A. Lan, X. Wang, and T. Zhang, Construction of Thiadiazole-Bridged sp²-Carbon-Conjugated Covalent Organic Frameworks with Diminished Excitation Binding Energy Toward Superior Photocatalysis, *J. Am. Chem. Soc.*, 2024, **146**, 1318–1325.
- S8. H. Liang, X. Bi, H. Chen, T. He, Y. Lin, Y. Zhang, K. Ma, W. Feng, Z. Ma, G. Long, C. Li, B. Kan, H. Zhang, O. A. Rakitin, X. Wan, Z. Yao and Y. Chen, A rare case of brominated small molecule acceptors for high-efficiency organic solar cells, *Nat. Commun.*, 2023, **14**, 4707.